Title

PRELIMINARY CALCULATIONS OF THE EFFECTS OF AIR AND LIQUID WATER-DRILLING ON MOISTURE CONDITIONS IN UNSATURATED ROCKS

Authors

Bodvarsson, G.S.
Niemi, A.
Spencer, A.

Publication Date

1988-11-01

LBL-25073
UC-403

Lawrence Berkeley Laboratory
UNIVERSITY OF CALIFORNIA

EARTH SCIENCES DIVISION

Preliminary Calculations of the Effects of Air and Liquid Water-Drilling on Moisture Conditions in Unsaturated Rocks

G.S. Bodvarsson, A. Niemi, A. Spencer,
and M.P. Attanayake

November 1988

Prepared for the U.S. Department of Energy under Contract Number DE-AC03-76SF00098.

DISCLAIMER

LBL-25073

Preliminary Calculations of the Effects of Air and Liquid Water-Drilling on Moisture Conditions in Unsaturated Rocks

G. S. Bodvarsson, A. Niemi, A. Spencer, and M. P. Attanayake

Earth Sciences Division
Lawrence Berkeley Laboratory
1 Cyclotron Road
Berkeley, California 94720

November 1988

This work was carried out under U.S. Department of Energy Contract No. DE-AC03-76SF00098 via the DOE-Nevada Office in cooperation with USGS, Denver.

Abstract

Numerical simulation studies are performed to investigate the effects of air and liquid water drilling on the time-dependent moisture conditions in nearby fractures and rock matrix blocks. The results obtained suggest that drilling with liquid water will increase the liquid saturation in the matrix by one or two percentage points after one year of recovery. For the characteristic curves used, this corresponds to a 10 to 20 percent increase in the relative permeability of the liquid phase. The results also indicate that air drilling has negligible effects on the moisture conditions within the matrix blocks.

Table of Contents

List of Figures

Acknowledgments

The authors appreciate technical review by K. Pruess and C. Doughty of LBL and E. Kwicklis of USGS, Denver, and also thank K. Pruess for allowing the use of TOUGH and GMINC for their work. This work was carried out under U.S. Department of Energy Contract No. DE-AC03-76SF00098 via the DOE-Nevada Office in cooperation with USGS, Denver.

INTRODUCTION

At the request of the United States Geological Survey (USGS), the Earth Sciences Division of Lawrence Berkeley Laboratory (LBL) has conducted limited numerical studies of the effects of air and liquid-water drilling on moisture conditions in unsaturated rocks. Decisions must be made to determine which drilling fluid should be used in the drilling of boreholes associated with the exploratory shaft at Yucca Mountain and whether dry or wet mining should be used in the excavation of underground chambers. It is of interest to use simplified models to obtain order of magnitude estimates of the disturbance to in-situ moisture conditions when gas or liquid water are used as drilling fluids.

The basic problem of water flow in fractures being drawn into the matrix by capillary forces has been studied by Travis et al. (1984) and Wang and Narasimhan (1986). Travis et al. (1984) showed that the effects of capillary suction are strong and greatly retard the advancement of the liquid front in the fractures. Wang and Narasimhan (1986) concluded that due to the strong capillary forces the liquid front would become sharp very quickly with rather uniform saturation profiles developing in the fractures and the matrix. These results are probably due to their use of harmonic weighting to evaluate the liquid mobility at interfaces between grid blocks. This will be discussed further in a later section.

Several previous studies have addressed the question of the effects of wet mining and drilling with liquid water on moisture contents of fractures and rock matrix blocks in the vicinity of the activity. Peters and Gauthier (1986) modeled the response of a matrix block to drilling with liquid water under relatively high pressure (20 m head). They investigated the conditions in the matrix block after drilling times varying from 1 to 100 minutes. They found that the liquid water migrates very short distances in the rock matrix, less than 5 m. They also found that water redistribution after drilling ceased was rather rapid, as the initial conditions were practically reached after a few minutes. For later reference it should be noted that the

authors used a harmonic mean weighting scheme for the mobilities at interfaces between grid blocks.

Kwicklis and Hoxie (1987) used a fracture-matrix model to investigate the effects of liquid-water drilling. They assumed a vertical fracture with a 24-micron aperture and the corresponding cubic law permeability, fracture characteristic curves similar to those for coarse sand, and a pressure head of 20 m for a 1 hour time period. They found that the water front moved approximately 2 m down the fracture after 1 hour of drilling. If a larger 240-micron fracture aperture was assumed, the water front moved more than 50 m. They also found that the redistribution of the moisture after drilling was quite rapid. Furthermore, they concluded that the numerical solution was quite sensitive to the grid spacing used. In their studies Kwicklis and Hoxie used an upstream weighting scheme for computing permeabilities at interfaces between grid blocks.

Montazer et al. (1987a) discuss the effects of dry versus wet mining on the hydrological conditions near underground chambers. They argue that minimally perturbed conditions are required if meaningful results are to be obtained from the infiltration and bulk-permeability tests. They stress the importance of these tests for obtaining combined characteristic curves for the fracture-porous rocks. They conclude that dry-mining techniques should be used in the mining of the infiltration and bulk-permeability test rooms. However, recent changes in the design of these tests may minimize the effects of the drilling fluid (E. Kwicklis, personal communication, 1988).

In the present work a coarse model is used to investigate the effects of gas and liquid-water drilling on fracture and matrix hydrological conditions. Lateral water migration during drilling and the effects of various mobility weighting schemes (harmonic, arithmetic and upstream weighting) at grid block interfaces are briefly investigated. All of the simulations were performed using upstream weighting unless noted otherwise. A fracture-matrix model similar to that used by Kwicklis and Hoxie (1987) is employed in the studies. It should be noted that very coarse spatial discretization is used, hence, the results obtained are only rough

approximations.

PROBLEM SPECIFICATION

In this work the basic model shown in Figure 1 was used. It consists of vertical fractures surrounding a matrix block on all sides. This simplified model approximately represents the case of a horizontal borehole intersecting near-vertical fractures. In a few cases horizontal fluid migration was studied by rotating the basic model 90° and assuming that horizontal fractures are the main fluid conduits. These cases represent the first attempt to study horizontal water migration from the shaft and excavated rooms using wet mining.

In the horizontal plane the matrix was discretized using the MINC method developed by Pruess (1983). A logarithmic grid spacing was used in the matrix with a 1 mm element adjacent to the fracture, increasing to 27 cm for the innermost element.

The fracture spacing was assumed to be 0.6 m based upon reported fracture densities of about 8-40 fractures per cubic meter for the Topopah Springs welded unit (Montazer and Wilson, 1984). A very coarse vertical grid spacing was used, with a 1.5 m element at the top of the system, increasing in size to a 15 m element at the bottom of the system; altogether a 50 m thick block was modeled. Limited sensitivity studies were conducted on the effects of the vertical gridding.

The parameter values used for most of the simulations are summarized in Table 1. For most of the simulations the rock matrix characteristic curves used were those proposed by Rulon et al. (1986) for the Topopah Springs member (USGS curves). The fracture characteristic curves were those used by Rulon et al. (1986), with relative permeability and matrix potential assumed to be exponential functions of liquid saturation. These fracture characteristic curves were derived using a parallel plate model and capillary theory (Montazer et al., 1987b). It should be noted that few measurements are available regarding the characteristic curves, hence, the results obtained are only first order estimates.

An air entry value of 0.0134 bars was used, yielding a fracture aperture of about 100

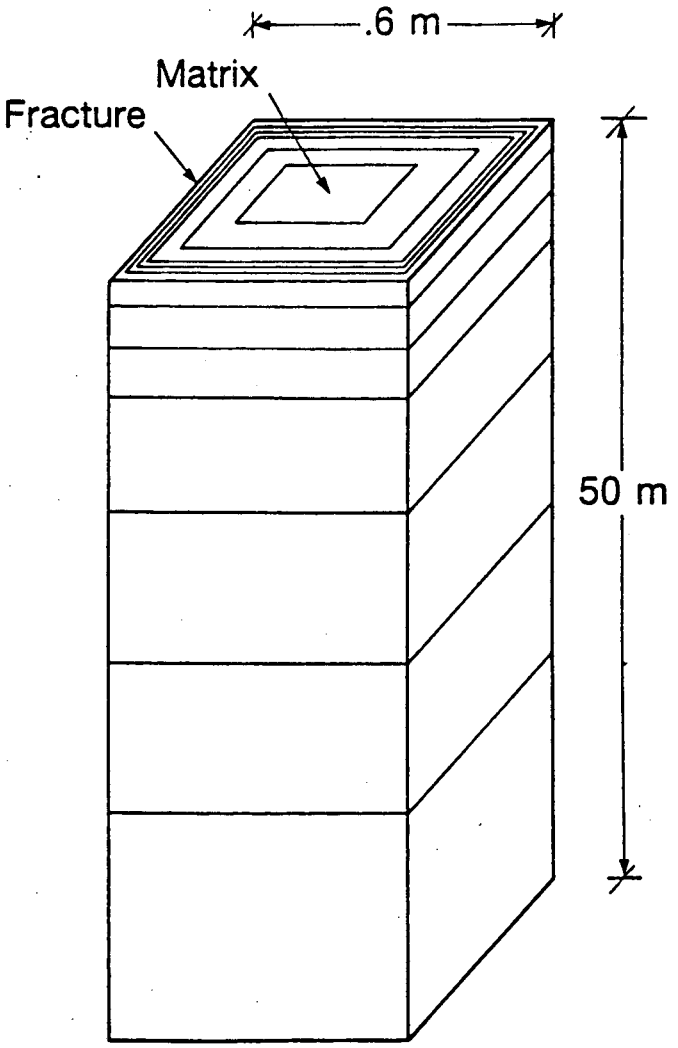

Horizontal discretization (m)

.0001 (fracture), .001,.005,.01,.05,.1,.134

Vertical discretization (m)

1.5, 2.5, 4.0, 7.0, 10.0, 10.0, 15.0

Figure 1. Discretized flow region used in the simulations.

microns as determined from a capillary rise equation. This fracture aperture was used for determining both the fracture permeability (through the cubic law) and the fracture volumes and interface areas; that is, the volumetric aperture was assumed to be similar to the hydraulic one.

One case study was carried out using the matrix and fracture characteristic curves for the Topopah Spring welded unit proposed by Klavetter and Peters (1986; Sandia curves). The relevant van Genuchten parameters for these characteristic curves are also given in Table 1. Figures 2 and 3 show the capillary pressure and liquid relative permeability versus liquid saturation, respectively, for USGS and Sandia characteristic curves.

Stable initial conditions were established by infiltrating a flux equivalent to 0.1 mm per year of liquid water through the system. Using the USGS characteristic curves, this resulted in uniform initial liquid saturations of 0.69 and 1.6×10^{-4} for the matrix and the fracture, respectively. Using the Sandia characteristic curves, initial matrix saturation was 0.80, and fracture saturation was approximately equal to the residual saturation. In both cases the capillary pressures in the matrix and the fracture were in equilibrium, with a uniform value of about -0.97 bars for the USGS curves and about -14.6 bars for the Sandia curves. This liquid flux was turned off during drilling but re-established during the recovery period.

During drilling, a water head equivalent to 20 m (2.0 bars) was imposed at the top of the system. At the lower boundary the initial pressure potential was maintained at all times. For most of the cases this boundary condition did not affect the results significantly. For the case in which the effects of lateral fluid movement due to capillary forces were investigated, the entire flow domain was rotated 90° to a horizontal position and the same water head of 20 m was applied to one side. In this case gravity effects were turned off and the entire system was initialized with the same matrix potential ($\approx$ -0.97 bars). In most cases drilling was assumed to last 12.25 minutes, after which the redistribution of moisture was computed for one year.

In the case involving gas drilling, a 2 bar air pressure was maintained at the top of the system. This value is probably low, as air pressure closer to 5 bars may be used in the air

Table 1. Parameter Values[1] Used in the Simulations

Matrix	
• porosity	$\phi_m = .12$
• absolute permeability	$k_m = 3.9 \cdot 10^{-18}$ m^2
• capillary pressure[2]	$\psi_m = \frac{1}{\alpha}[(\frac{S_e - S_r}{S - S_r})^{\frac{1}{m}} - 1]^{\frac{1}{n}}$; with the van Genuchten parameters $S_e = .984$, $S_r = .318$, $\alpha = 1.147$ bar^{-1}, $m = .671$, $n = 3.040$
• relative permeability[2]	$k_{rl} = \left[\frac{S - S_r}{S_e - S_r}\right]^{1/2}\left\{1 - \left[1 - \left[\frac{S - S_r}{S_e - S_r}\right]^{1/m}\right]^m\right\}^2$ or $k_{rl} = \frac{\left\{1 - (\alpha\lvert\psi\rvert)^{n-1}[1 + (\alpha\lvert\phi\rvert)^n]^{-m}\right\}^2}{[1 + (\alpha\lvert\phi\rvert)^n]^{m/2}}$ with van Genuchten parameters as above
Initial Conditions[3,7]	
• capillary pressure	$\psi_m = -.968$ bars
• liquid saturation	$S_m = .691$
Fracture	
• aperture[4]	$\delta_f = .1$ mm
• porosity	$\phi_f = 1.$
• spacing	$D = .60$ m
• absolute permeability per fracture[5]	$k_f = 8.33 \cdot 10^{-10}$ m^2
• relative permeability[6]	$k_{rl} = S_l^{1.936}$
• capillary pressure[6]	$\psi_f = .0134 \cdot S_l^{-.491}$ bars
Initial Conditions[7]	
• capillary pressure	$\psi_f = -.968$ bars
• liquid saturation	$S_f = .164 \cdot 10^{-3}$

Notes:

1. Source Rulon et al. (1986), unless otherwise indicated.
2. (a) for the Sandia curves van Genuchten parameters; S_e=1, S_r=.08, α=.05787^{-1}, m=.4438, n=1.798 (Klavetter and Peters, 1986)
   (b) for the hysteretic case; $\alpha_{mainwetting} = 2.294$, $\alpha_{maindrying} = 1.147^{-1}$
3. Correspond to .1 mm/yr infiltration.
4. Fracture aperture corresponds to the air entry value = .0134 bar through the capillary rise equation (Wang and Narasimhan, 1985).

$$aev = \frac{2\gamma}{\delta_f \cdot \rho \cdot g}$$

   where $\gamma = .07$ kg/s^2, $\rho = 1000$ kg/m^3 and $g = 9.81$ m/s^2.
5. Permeability determined from cubic law; $k_f = (\delta_f)^2/12$.
6. For Sandia curves; van Genuchten curves with $S_e = 1$, $S_r = .0395$, $\alpha = 13.12$ 1/bars, $m = .7636$, $n = 4.23$.
7. For Sandia curves $\phi_m = \phi_f = 14.6$ bars, $S_m = .80$, $S_f = .038$.

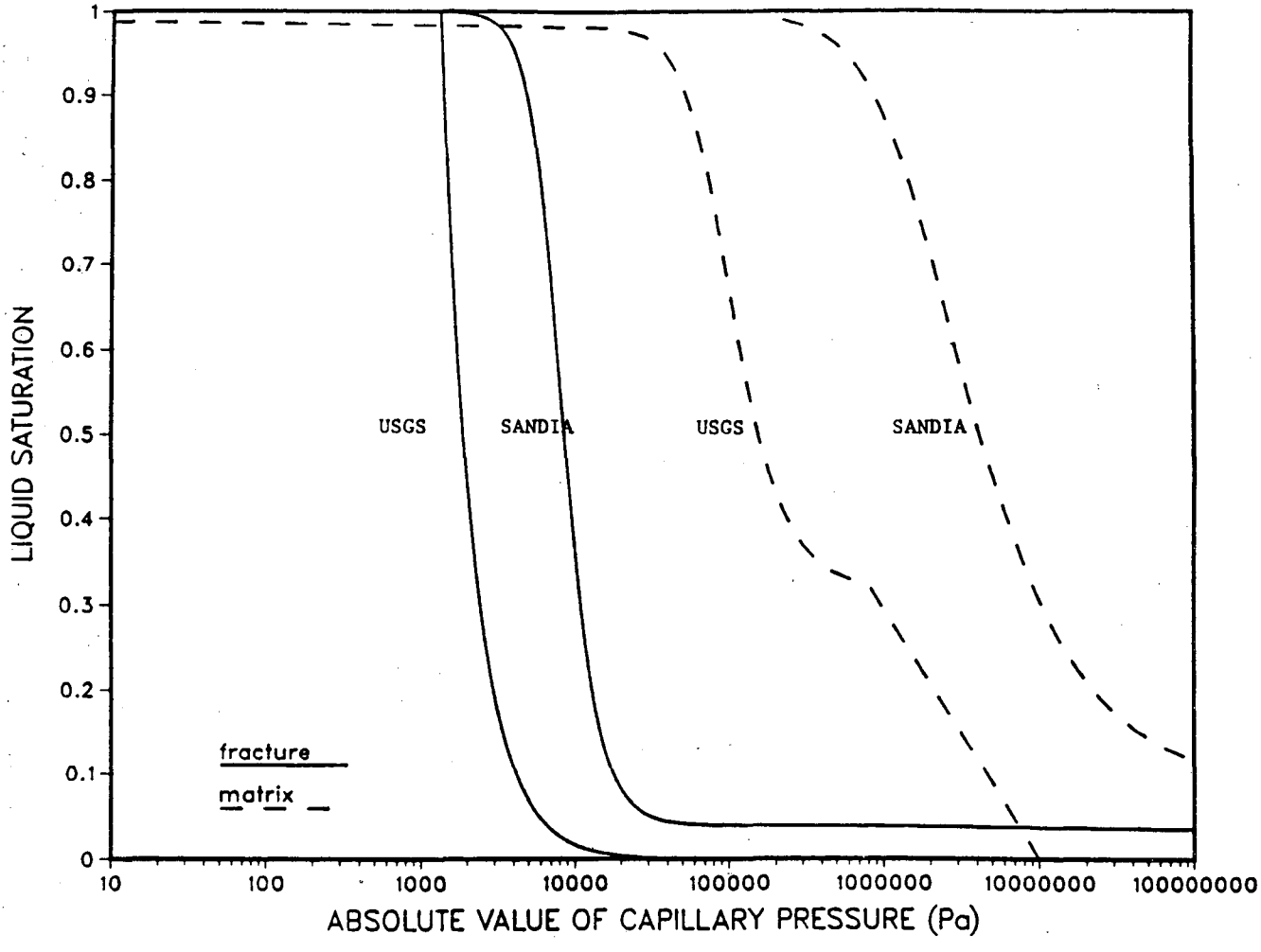

Figure 2. Capillary pressure-liquid saturation curves used in the simulations (Klavetter and Peters, 1986; Rulon et al., 1986).

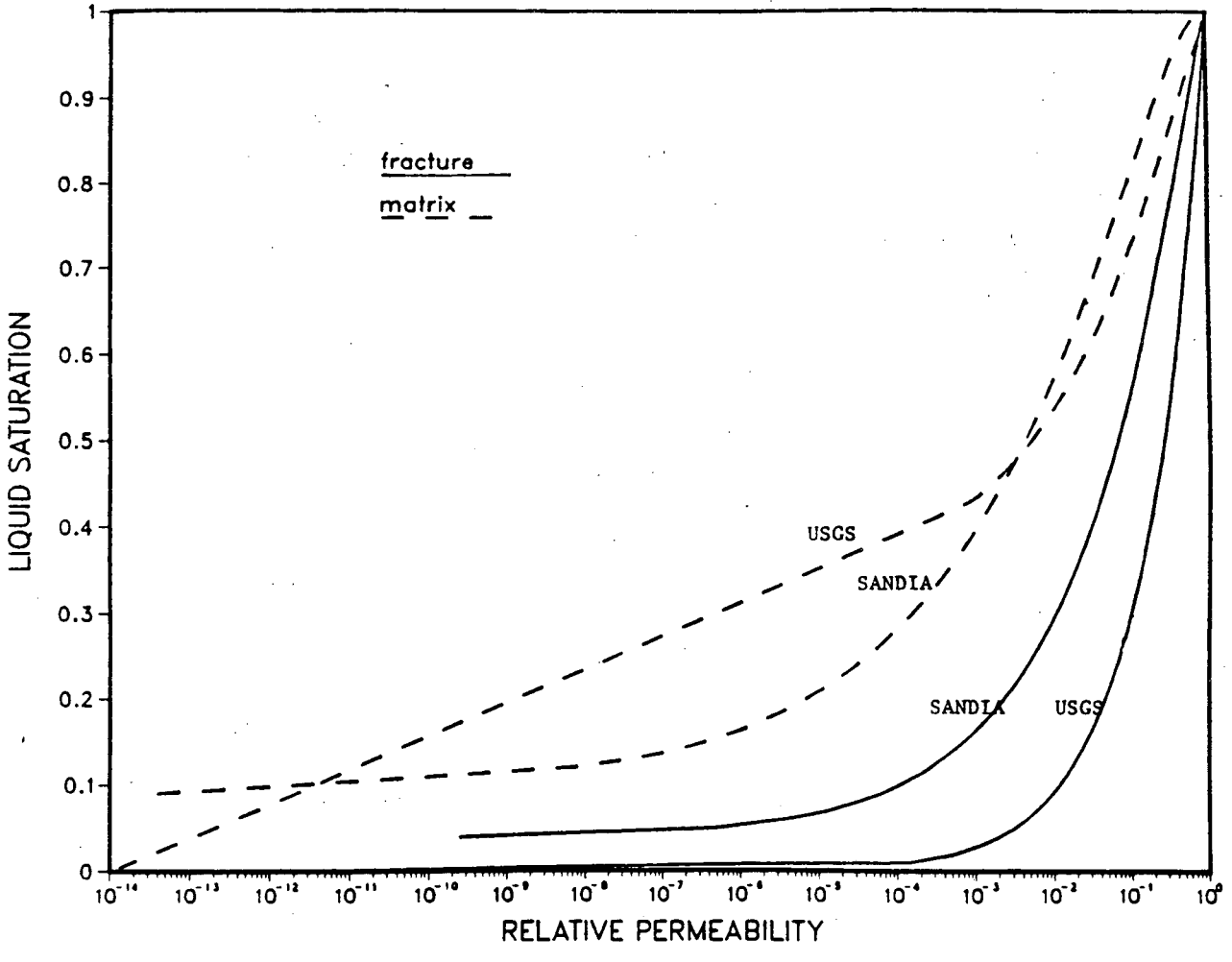

Figure 3. Relative permeability-liquid saturation curves used in the simulations (Klavetter and Peters, 1986; Rulon et al., 1986).

drilling (D. Hoxie, personal communication, 1988). Air movement was also computed for the liquid water drilling cases and was found to have practically no effects for the system modeled. In all cases the lower boundary was sufficiently deep that the specified constant pressure boundary condition did not affect the solution significantly. The simulations were carried out using the numerical code TOUGH (Pruess, 1987). An outline of all the simulations is given in Table 2.

RESULTS

USGS Characteristic Curves

In the first set of simulations the USGS characteristic curves were used. Figures 4 through 8 show some of the results obtained. Figures 4 and 5 show the liquid saturation profiles for the fracture and the rock matrix (0.5 mm from the fracture), respectively, after 12.25 minutes of drilling and for selected times during the subsequent recovery. A 12.25 minute drilling period was used as an estimate for the time it takes to drill past an open vertical fracture. At the end of drilling the matrix is near saturation in the top 7.5 m; below that the liquid saturation decreases monotonically to the initial value of 0.69 at 20 m depth. In the fracture, large increases in liquid saturation occur to about 7.5 m depth at the end of drilling (Figure 4). Below this depth the liquid saturation increases significantly to a depth of about 11.5 m, although the scale used in Figure 4 is too coarse for this to be seen. The liquid saturation in this region has increased by more than an order of magnitude (from 1.6×10^{-4} to $> 10^{-3}$), thus greatly decreasing the magnitude of capillary pressure. Hence, fluid flow into the rock matrix causes the observed increase in liquid saturation there. The apparent greater vertical penetration of the disturbance in the matrix (Figure 5) compared to the fracture (Figure 4) is therefore caused by the coarse grid and the characteristic fracture curves used.

After drilling stopped, the fracture recovered almost to its initial moisture content within hours (Figure 4). Most of the fluids within the fracture were drawn into the matrix by capillary force. Hence, the front did not advance significantly farther along the fracture after the

Table 2. Summary of Simulations

	Case	Comments
Effect of characteristic curves	1 2 3	USGS - curves Sandia - curves hysteresis
Grid effects	4 5	"coarse" grid "fine" grid
Effect of the weighting scheme	6 7 8	upstream weighting arithmetic mean weighting harmonic mean weighting
Horizontal moisture migration	9 10	0.1 mm fracture 0.05/0.01 mm fracture
Air drilling	11	2 bar air pressure boundary condition

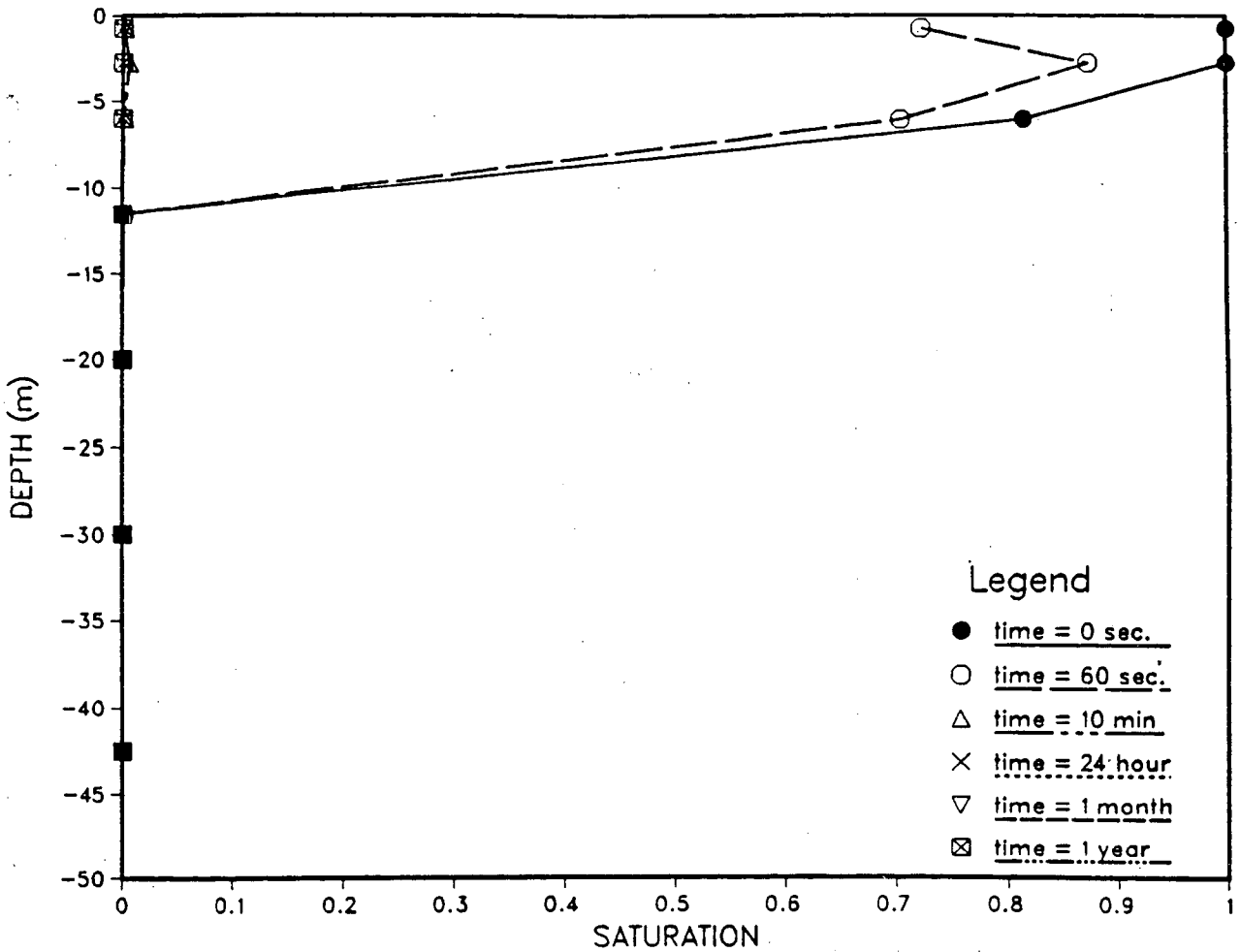

Figure 4. USGS characteristic curves: Liquid saturation in the fracture for various recovery times.

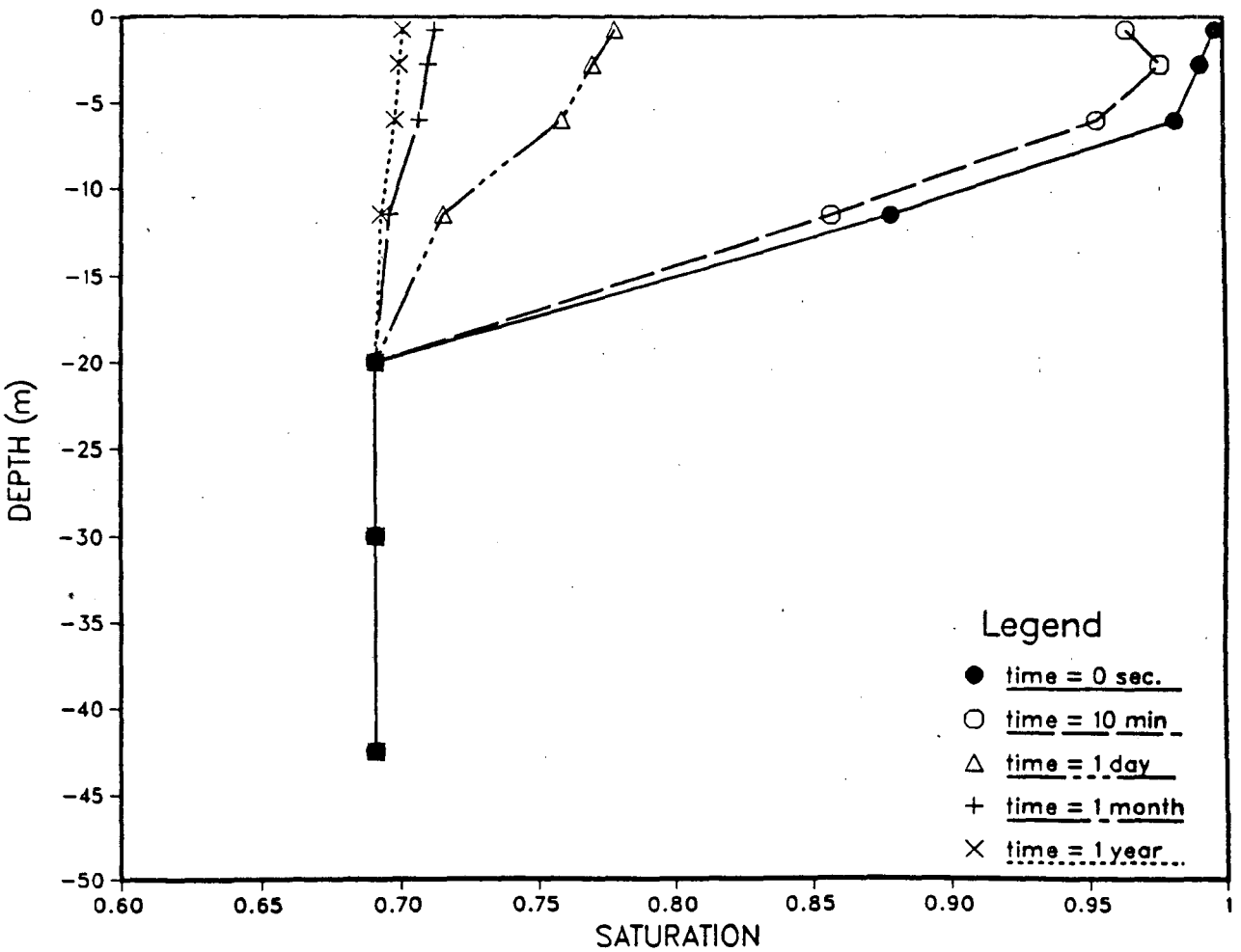

Figure 5. USGS characteristic curves: Liquid saturation in the matrix (0.5 mm from the fracture) for various recovery times.

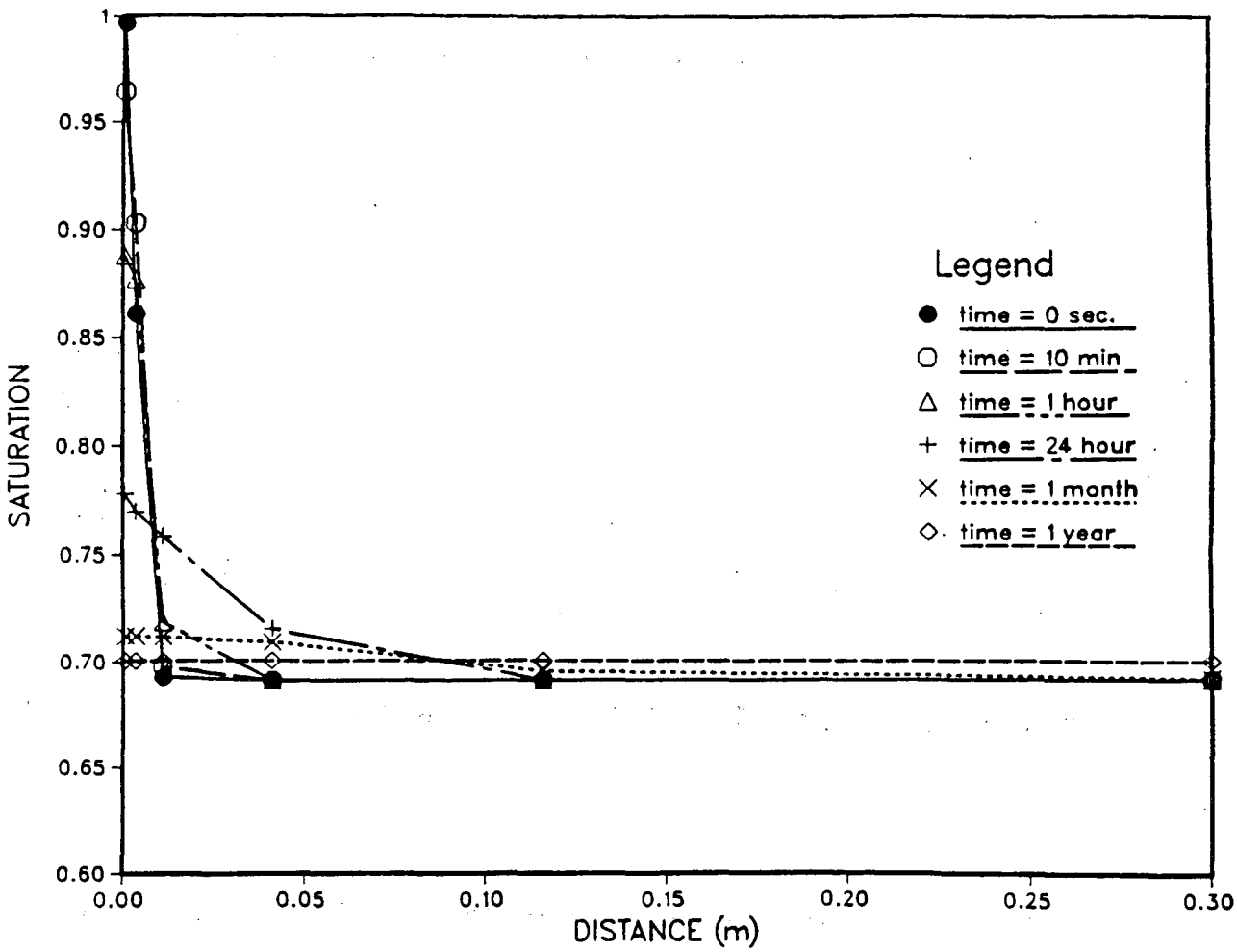

Figure 6. USGS characteristic curves: Liquid saturation in the matrix at a depth of 0.75 m for various recovery times.

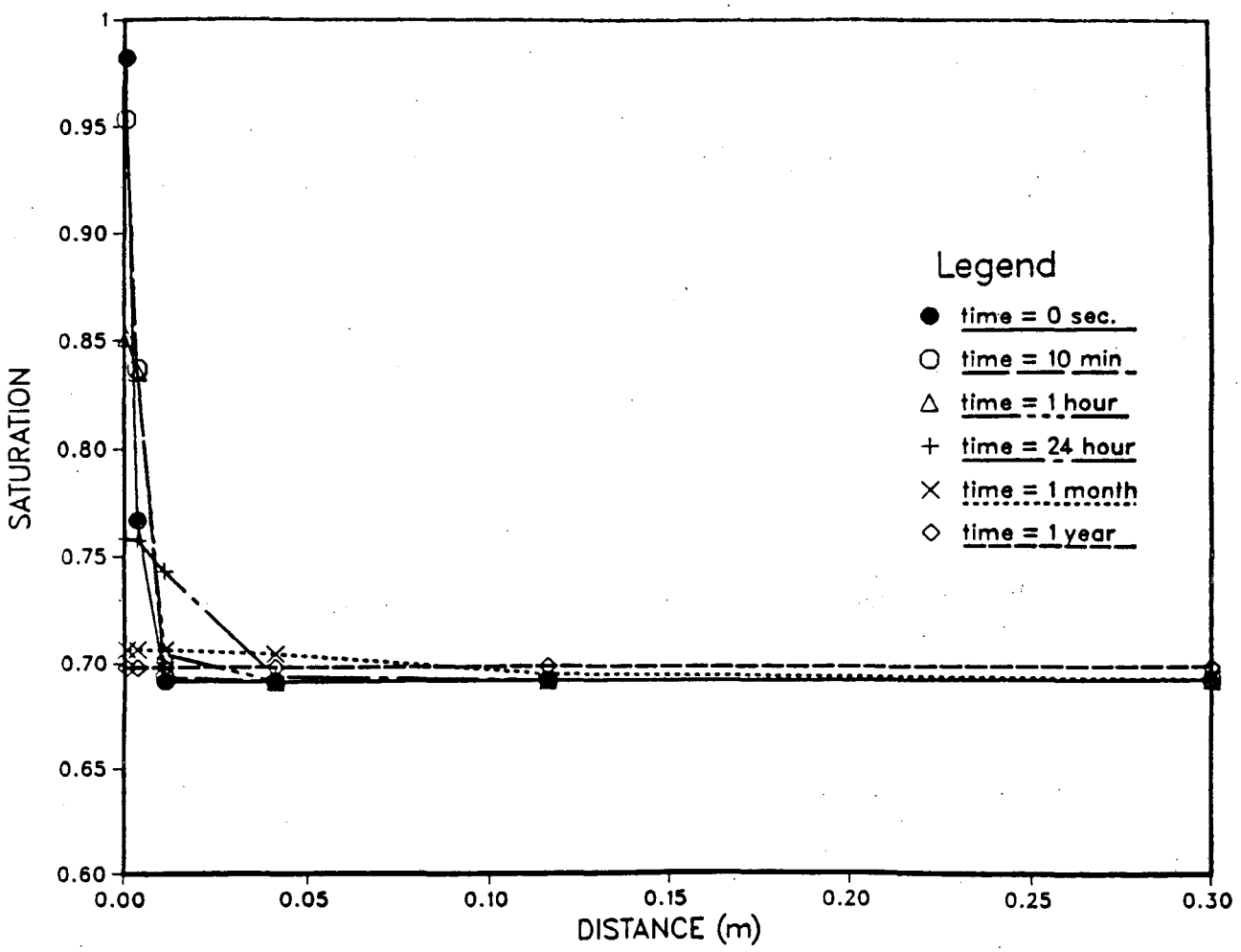

Figure 7. USGS characteristic curves: Liquid saturation in the matrix at a depth of 6 m for various recovery times.

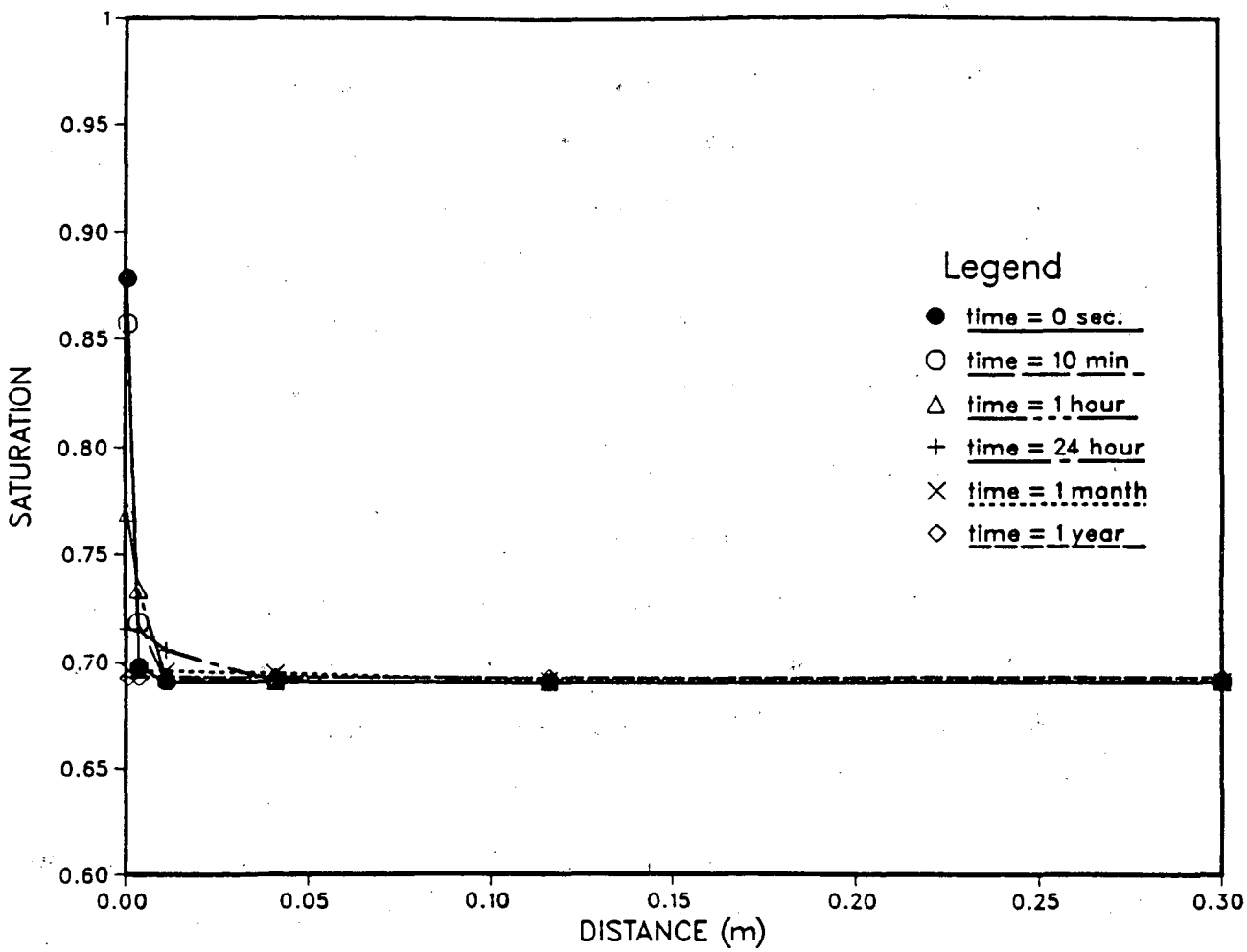

Figure 8. USGS characteristic curves: Liquid saturation in the matrix at a depth of 11.5 m for various recovery times.

constant head boundary condition was removed. This behavior was also observed by Kwicklis and Hoxie (1987) in their numerical calculations. The moisture redistribution in the rock matrix took much longer than in the fracture because of the low permeability of the rock matrix (microdarcies). Figure 5 shows that rapid moisture redistribution occurred during the first month of recovery, with the liquid saturation recovering to within two percentage points of the initial liquid saturation.

Figures 6 through 8 show that the main mechanism of moisture redistribution is continued capillary suction into the rest of the matrix block until a quasi-equilibrium in capillary pressure is achieved. After one month of recovery the liquid saturation differs by up to two percentage points from the initial value, which corresponds to a 23% change in the liquid relative permeability. After one year of recovery the maximum difference is about one percentage point, which corresponds to a maximum increase of 10% in the liquid relative permeability.

Sandia Characteristic Curves

The same problem was investigated using the Sandia characteristic curves (Klavetter and Peters, 1986; see Table 1). For a 0.1 mm/year flux these characteristic curves yield a liquid saturation of about 80% in the matrix. Assuming a capillary pressure equilibrium between the fracture and the matrix yields a fracture liquid saturation in the range of the residual saturation. The results obtained are shown in Figure 9 through 12. Figures 9 and 10 show that the liquid front migrates about 12 m down the fracture and to a similar depth in the matrix elements closest to the fracture (0.5 mm away from the fracture). The results using the Sandia curves are very similar to those obtained using the USGS curves, with a maximum of 1.9 percentage points difference in saturation between the initial value (80%) and that obtained after a recovery of 1 month, depending upon the depth of observation within the matrix. This corresponds to a maximum of about 20% difference in the relative permeability of the liquid phase.

During the recovery period between one month and one year, the liquid saturations changed only slightly. This is because after one month of recovery the horizontal moisture

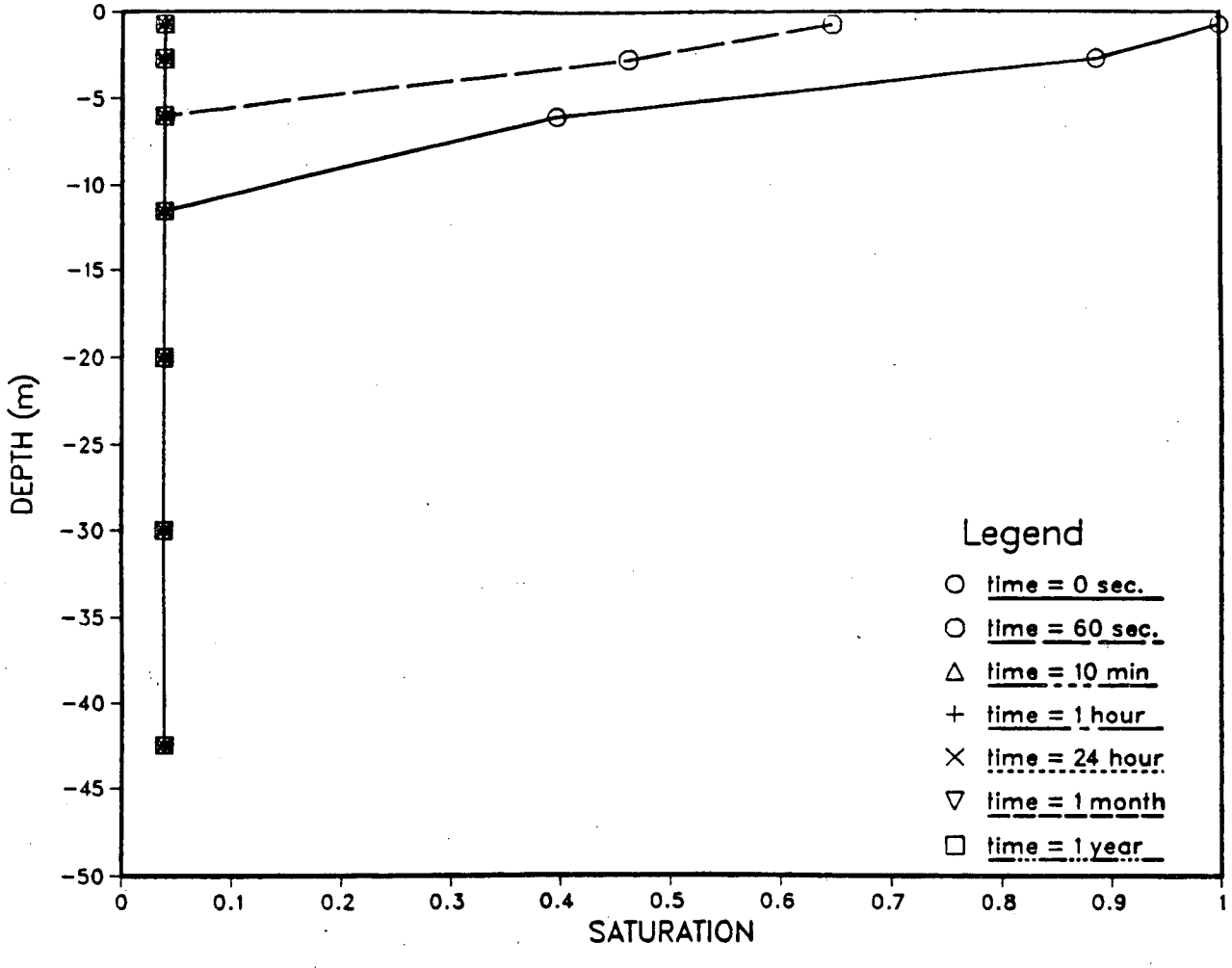

Figure 9. Sandia characteristic curves: Liquid saturation in the fracture for various recovery times.

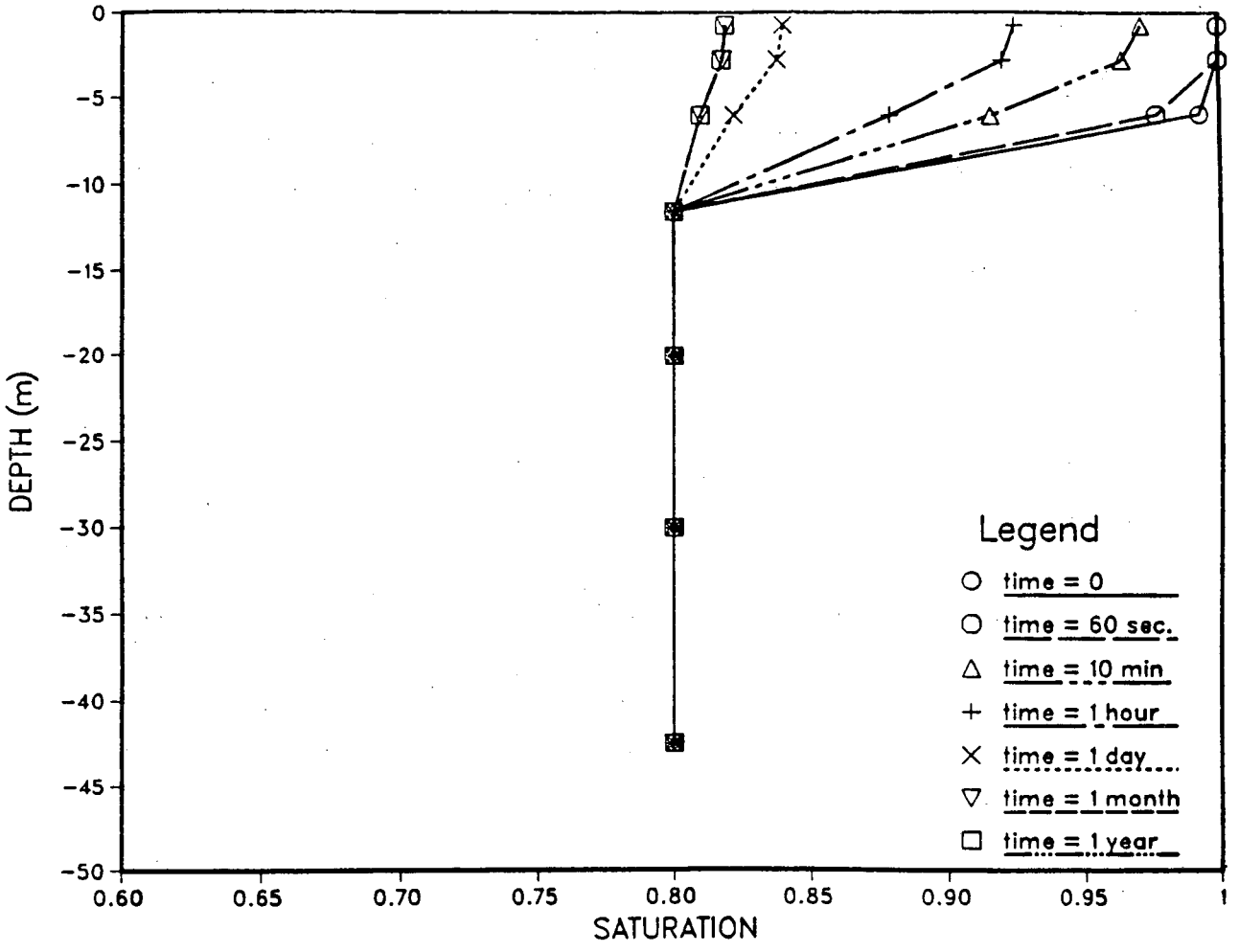

Figure 10. Sandia characteristic curves: Liquid saturation in the matrix (0.5 mm from the fracture) for various recovery times.

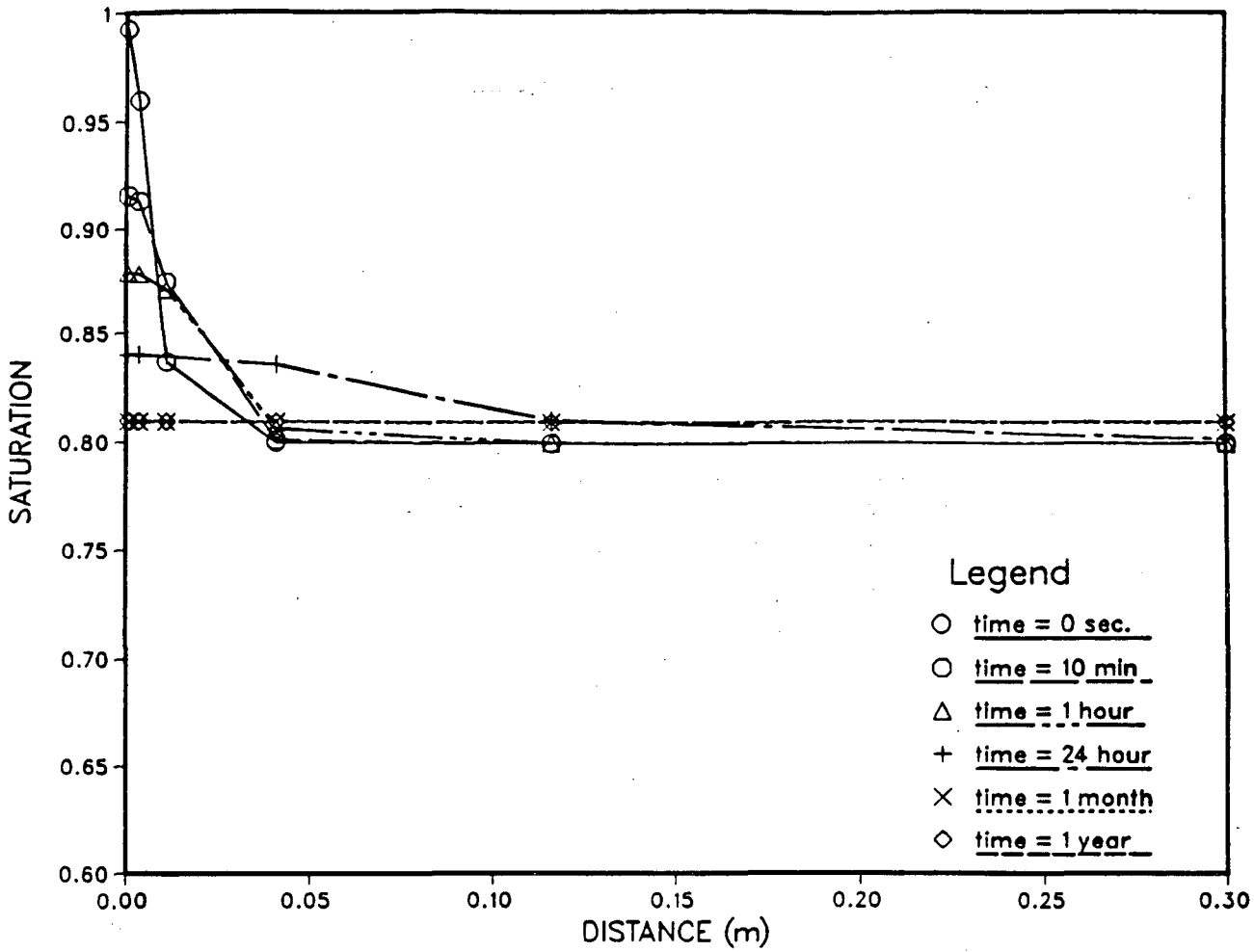

Figure 11. Sandia characteristic curves: Liquid saturation in the matrix at a depth of 0.75 m for various recovery times.

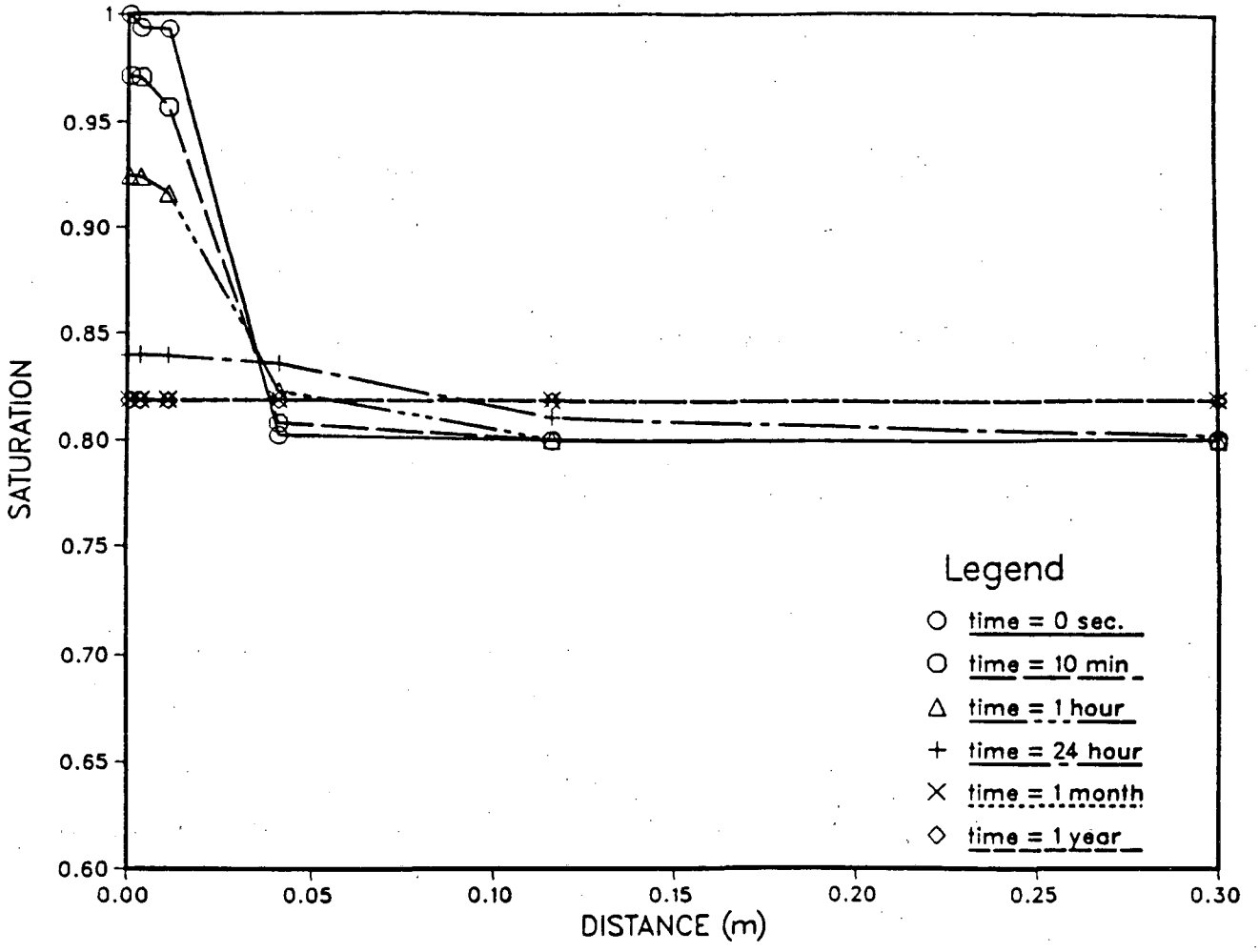

Figure 12. Sandia characteristic curves: Liquid saturation in the matrix at a depth of 6 m for various recovery times.

redistribution in the matrix has already occurred, hence, the only changes in liquid saturations are due to slight downward migration of the moisture. This process, however is very slow because of the small matrix permeability. The coarse grid used may also reduce the vertical moisture migration.

Hysteretic Capillary Pressure-Liquid Saturation Relationship

A brief sensitivity study was conducted on the effects of hysteresis in the matrix capillary pressure-liquid saturation relation on the moisture migration and redistribution. Hysteresis in the relative permeability-liquid saturation relation was neglected, which should not cause significant errors (see for example, Kool and Parker, 1987). It is also believed that hysteresis is more pronounced for the rock matrix than for the fractures (Montazer and Wilson, 1984). Because of this, we only considered hysteresis for the matrix; the fracture characteristic curves were assumed non-hysteretic. All the other parameter values used were those shown in Table 1 (USGS curves).

Since no actual hysteresis measurements for the welded units at Yucca Mountain are presently available, a theoretically derived hysteresis model was used. The model, which we have modified from the dependent domain model of Mualem (1984) and programmed into the numerical simulator TOUGH, computes the hysteretic scanning paths when the equations of the main wetting and main drying curves are known. Details of the model are given in Niemi et al. (1987). The USGS matrix curve was used as the main drying curve and a hypothetical wetting curve was predicted by using the ratio $\alpha_{wetting}/\alpha_{drying} = 2.0$ (where α is the van Genuchten parameter). This ratio was suggested by Kool and Parker (1987) for prediction of the difference between the main wetting and main drying curves for cases where data are lacking. Their results were based on experimental analyses conducted for different soils.

The resulting main wetting and main drying curves are shown in Figure 13. They are assumed to converge towards the same maximum liquid saturation. There is some experimental evidence (see for example, Kool and Parker, 1987), that the maximum liquid saturation on the main wetting curve is smaller than the corresponding one for the main drying curve. The

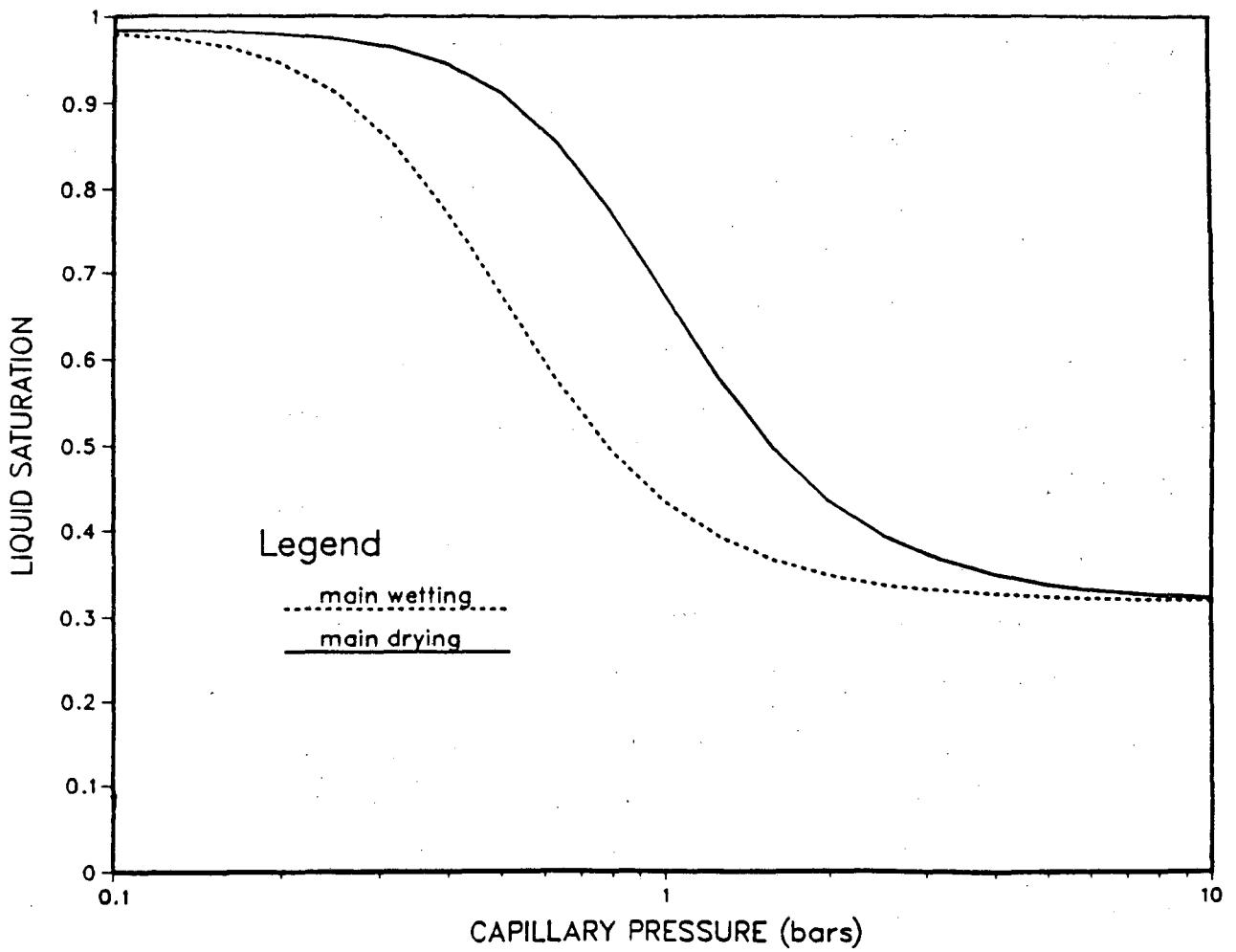

Figure 13. Hysteresis model: Main wetting and drying curves used.

lack of data on the magnitude of this difference for welded tuffs and the preliminary nature of our computation justifies the use of the same value for both.

The system was simulated by assuming a 12.25 minute drilling period followed by a one year recovery period. Initially, the system was assumed to be draining, hence, the main drying curve was used to determine the initial matrix conditions. The liquid saturation distributions in the fracture, in the matrix column immediately adjacent to the fracture, and in the uppermost layer of the matrix are shown in Figures 14, 15 and 16, respectively. Examples of the simulated hysteretic scanning paths for some grid blocks are shown in Figure 17.

Comparison of Figures 4 and 14 shows that the fracture liquid saturations at the end of drilling are somewhat higher in the hysteretic case than in the non-hysteretic case. This is probably the result of the lower matrix capillary suction in the hysteretic case (when a system wets along a first order wetting curve instead of the main drying curve, the same liquid saturation corresponds to a lower capillary pressure, as shown in Figure 17). An alternative explanation is the somewhat lower liquid relative permeability of the matrix in the hysteretic case (E. Kwicklis, personal communication, 1988). Higher fracture liquid saturations in the hysteretic case, also explain why further down (at ≈ 11.5 m) the matrix saturations are slightly higher in the hysteretic case than in the non-hysteretic case, in spite of the fact that at this level also capillary suctions were smaller in the hysteretic case. Parts of the matrix that were affected most during the drilling (grid blocks near the fracture in the upper layers) became fully saturated and their scanning paths thus converged with the main drying (and main wetting) curve. Partly because of this, the differences in matrix liquid saturation distributions between the hysteretic and non-hysteretic cases were not very significant at the end of the drilling (Figures 5 and 15).

A more significant difference was observed during the recovery period. Due to the lower matrix capillary suction in the interior of the matrix or alternatively lower matrix liquid permeability, the recovery was somewhat slower for the hysteretic case. This can be seen by comparing Figures 5 and 15. At the end of the 1 year recovery period the capillary pressure in

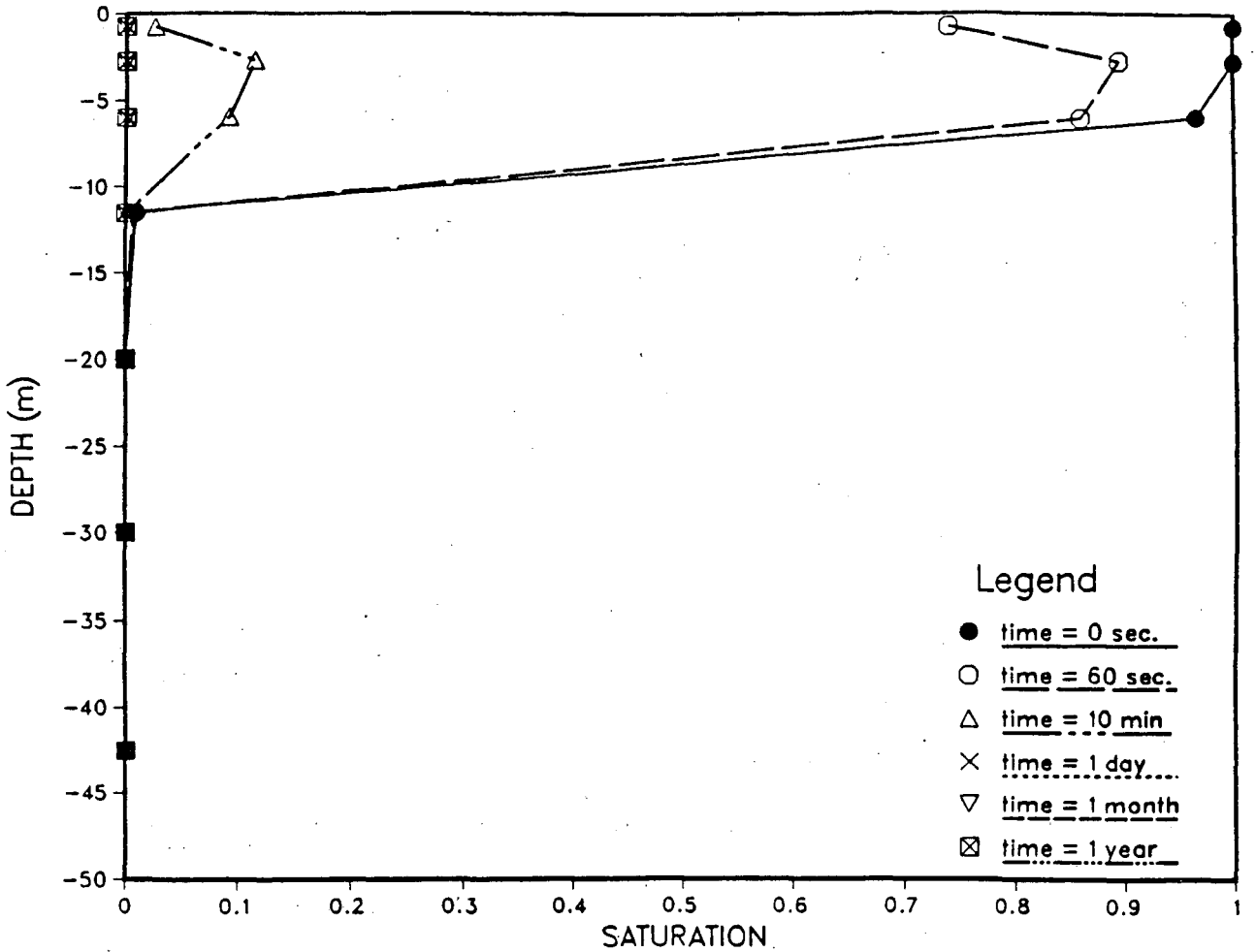

Figure 14. Hysteresis model: Liquid saturation in the fracture for various recovery times.

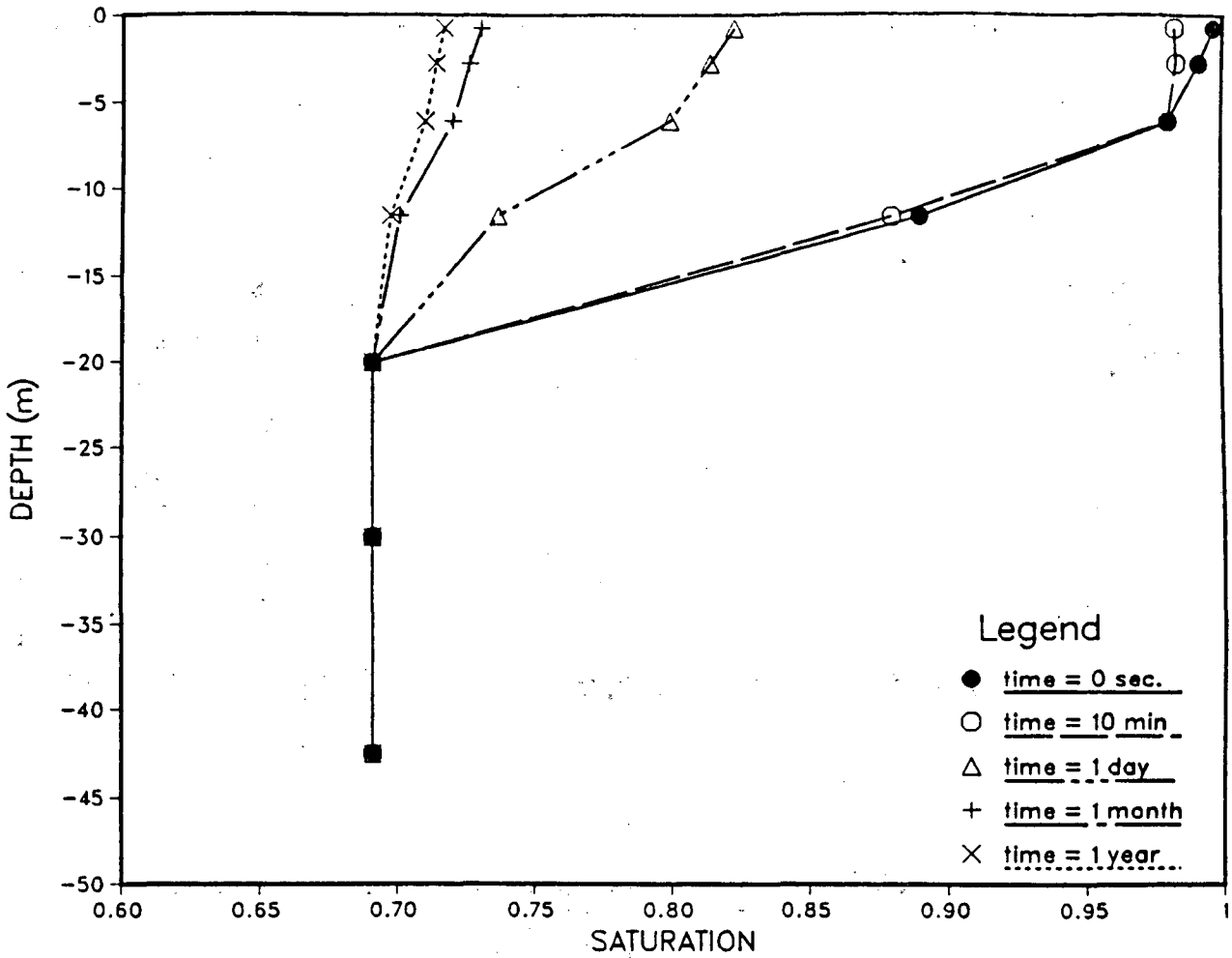

Figure 15. Hysteresis model: Liquid saturation in the matrix (0.5 mm from the fracture) for various recovery times.

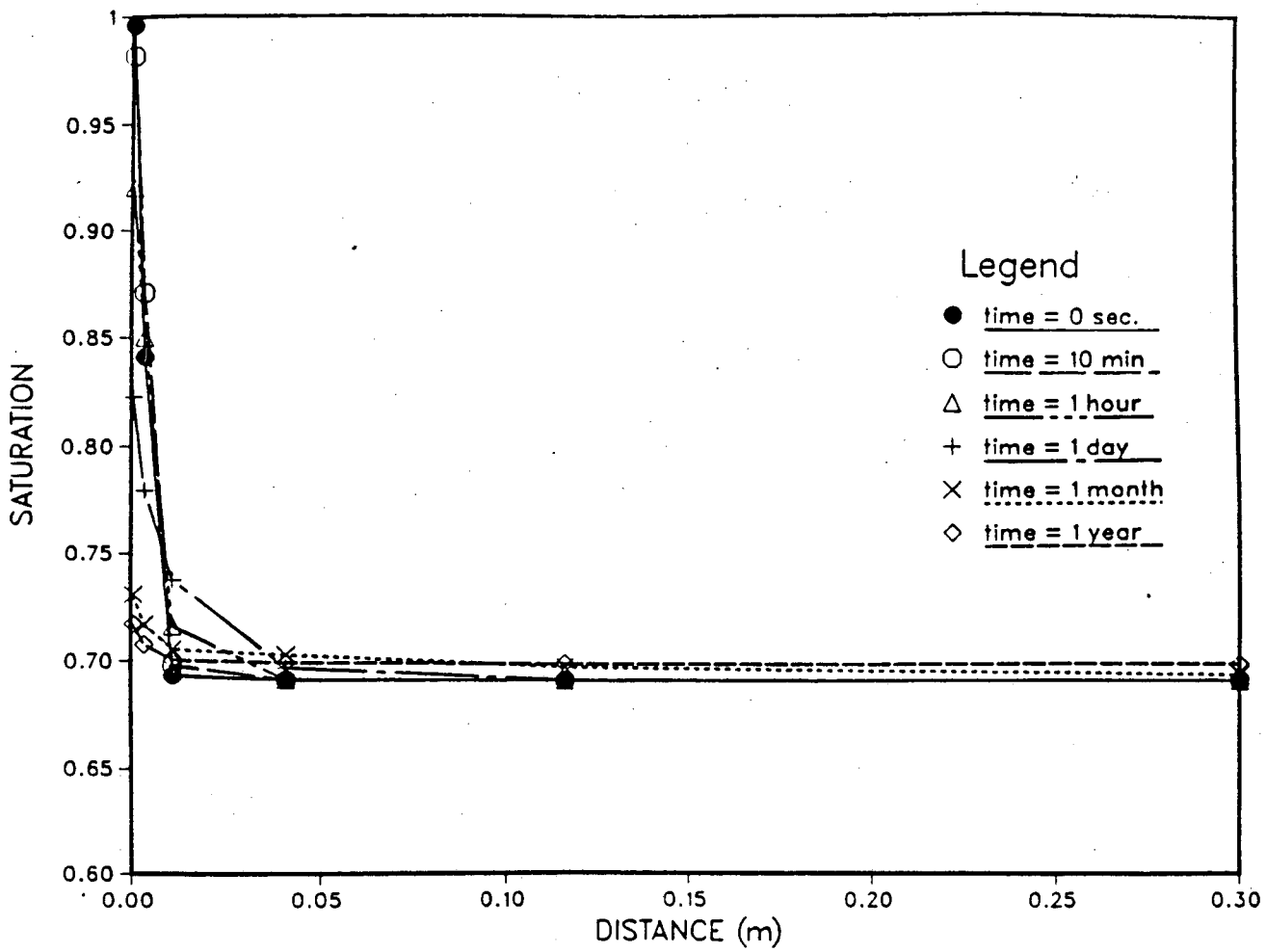

Figure 16. Hysteresis model: Liquid saturation in the matrix at a depth of 0.75 m for various recovery times.

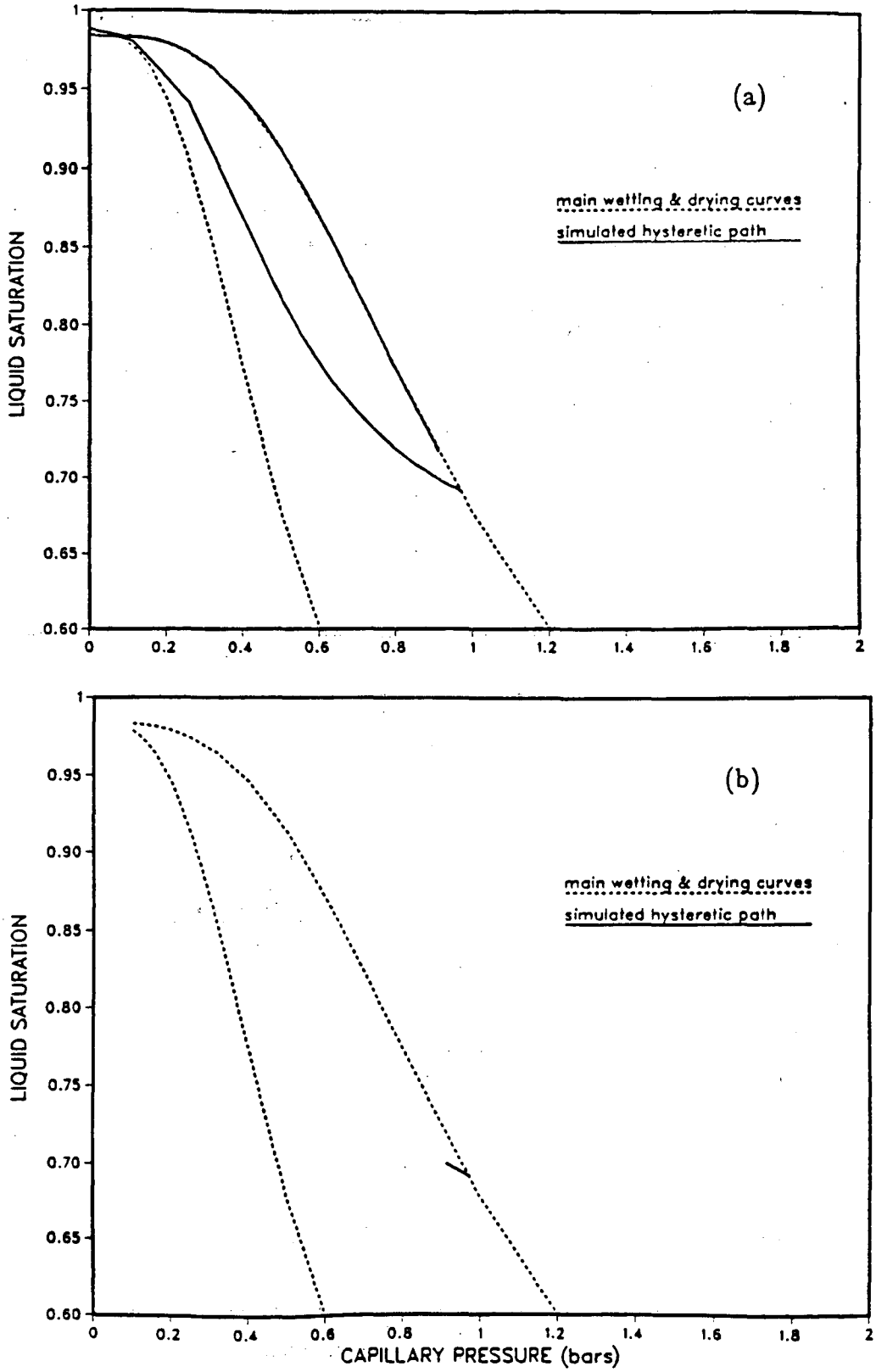

Figure 17. Hysteresis model: Hysteretic paths for various gridblocks. (a) 0.5 mm from the fracture, 0.75 m depth; (b) center of the matrix, 0.75m depth.

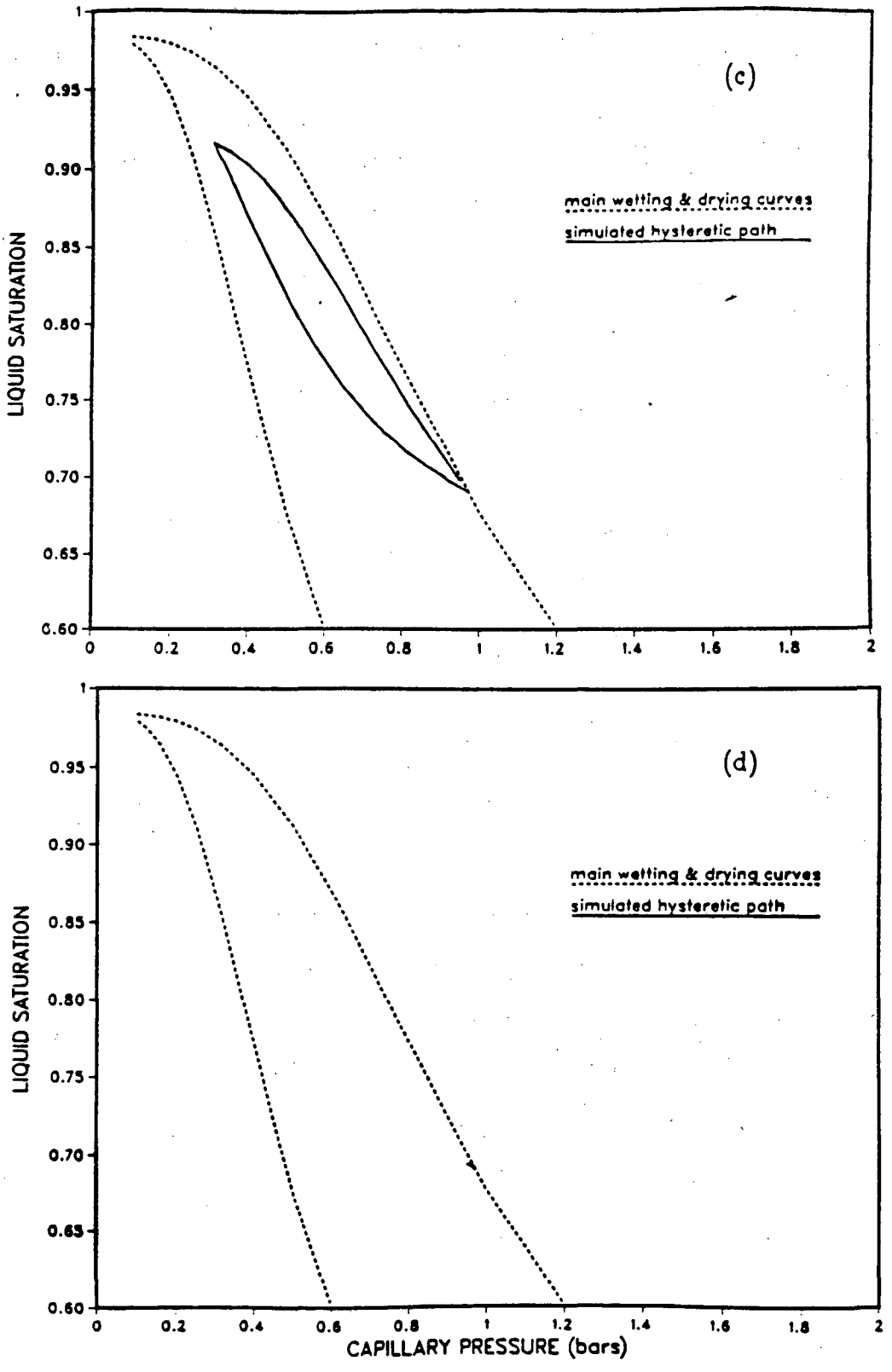

Figure 17. (Continued) Hysteresis model: Hysteretic paths for various gridblocks. (c) 0.5 mm from the fracture, 11.5 m depth; (d) center of the matrix, 11.5 m depth.

each matrix layer is uniform and in equilibrium with conditions within the adjacent fracture element. However, because of hysteresis, the liquid saturations were not uniform horizontally in the upper layers. This non-uniformity was most pronounced in the top matrix layer (Figure 16).

At the end of the recovery the matrix liquid saturations were within 2.6 percentage points of the initial liquid saturation in comparison to 1 percentage point for the non-hysteretic case. This corresponds to a maximum increase of 29% in the matrix relative permeability, in comparison to 10% for the non-hysteretic case.

Grid Effects

A limited sensitivity study was conducted on the effects of grid spacing on the moisture migration and distribution within the fracture and the rock matrix. The "coarse" grid spacing was identical to that used in the previous simulations (Figure 1). The "fine" grid was constructed by refining the coarse grid by a factor of three in the vertical direction, i.e., allowing three equally spaced elements for each element of the coarse grid. The horizontal gridding in the rock matrix remained the same.

The problem considered was very similar to the one discussed before, except that the fracture permeability was somewhat higher than in the earlier cases. A drilling period of five minutes was assumed, again with a water head of 20 m. Figures 18 and 19 show the moisture distributions in the fracture and the adjacent rock matrix (0.5 mm away from the fracture) during the recovery after drilling, for both the coarse and the fine grid. Figure 18 shows that there is a considerable difference between the results for the two grids in the fracture at the end of drilling. As expected, the coarse grid yields a more smeared front than the fine grid. In both cases the moisture leaves the fracture very quickly after recovery begins. In the rock matrix elements close to the fracture, there is also a considerable difference in the liquid saturation profiles at the end of the drilling. However, the behavior during the recovery period is very similar for the two grids as shown in Figure 19. Also, the time dependent flux into the fracture from the constant pressure upper boundary is very similar for both grids (Figure 20). This

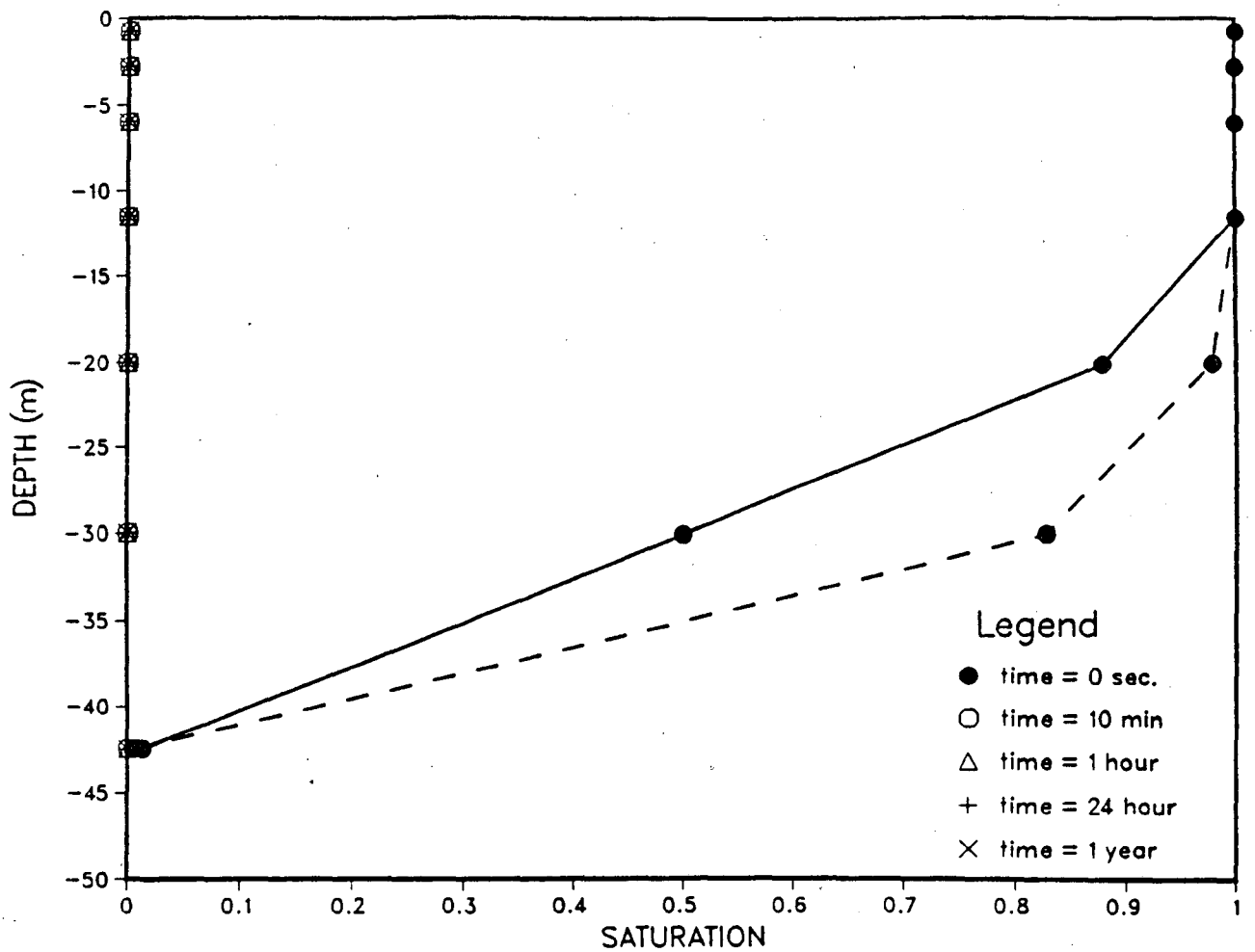

Figure 18. Grid effects: Liquid saturation profiles in the fracture for the coarse mesh (solid line) and the fine mesh (dashed line).

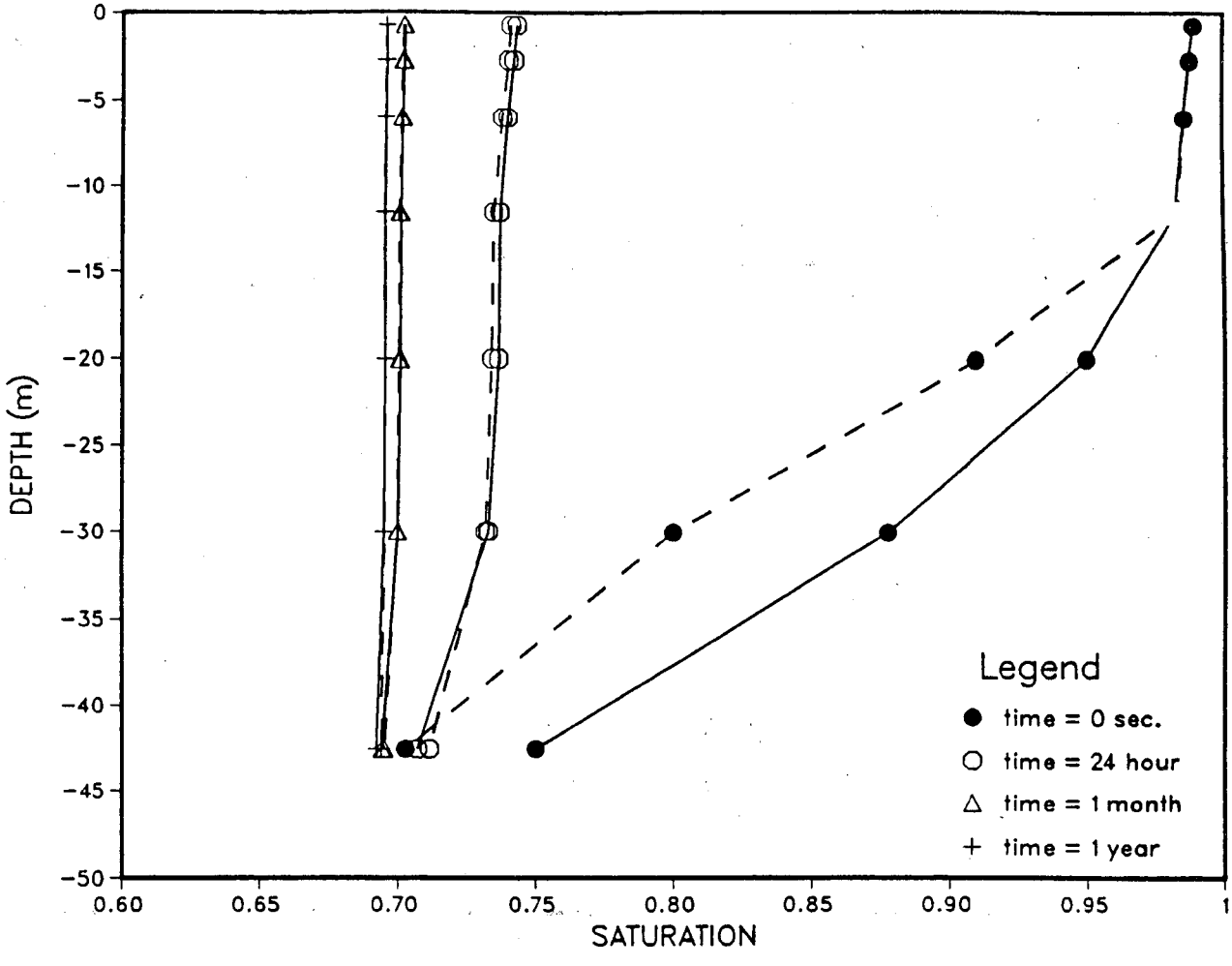

Figure 19. Grid effects: Liquid saturation profiles in the matrix (0.5 mm from the fracture) for the fine mesh (dashed line).

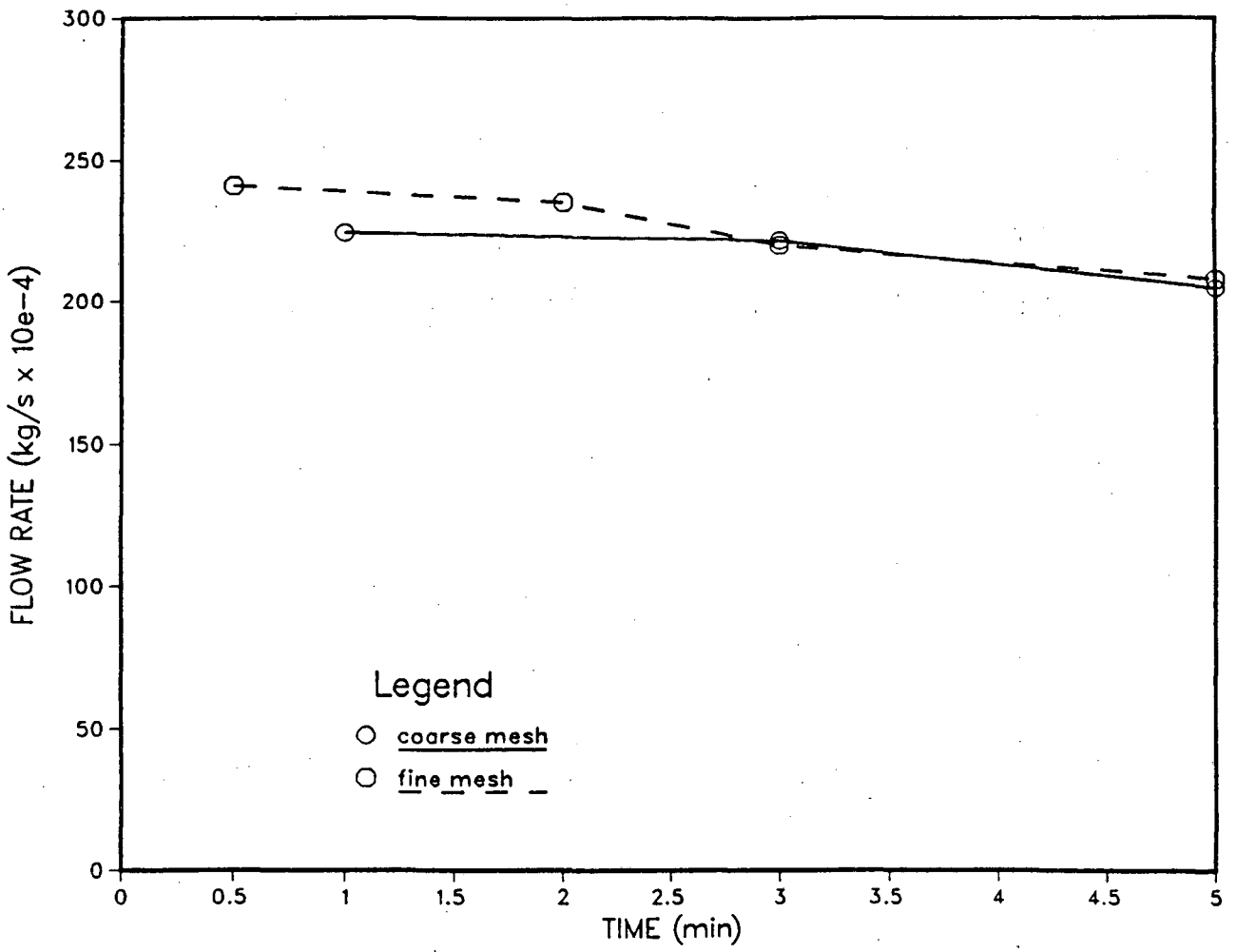

Figure 20. Grid effects: Flow into the top fracture element for the coarse mesh and the fine mesh.

limited sensitivity study suggests that the grid effects mainly affect the shape of the moisture front. They do not significantly affect the moisture redistribution and liquid saturations during the recovery period. As the long-term residual effects in the liquid saturations of the fracture and the matrix are of most importance in testing following drilling, the results suggest that the grid effects are secondary in importance.

Effects of Weighting Schemes

In numerical modeling of fluid, heat and chemical transport where spatial variations are present in fluid or rock parameters one must choose a rationale for averaging the parameters between grid blocks. For example, in problems involving unsaturated fluid flow, the effective permeability to both phases (liquid and gas) will vary spatially with the liquid saturation. In each grid block the liquid saturation is known and consequently the effective permeability associated with the grid block is known. However, the effective permeabilities for the two phases are needed at the interfaces between grid blocks in order to compute flow of gas and liquid between the two grid blocks. Various weighting schemes have been devised for estimating the interface values including those referred to as harmonic mean, upstream weighting and arithmetic mean weighting.

Figure 21 shows the equations used to compute the interface permeability for the harmonic, arithmetic and upstream weighting schemes. In the present study the harmonic mean permeability is obtained by computing the harmonic mean of the effective permeabilities of the grid blocks (kk_{rl}, where k is the absolute saturated permeability and k_{rl} is the relative liquid permeability). Similar weighting can be used for the gas phase. In both the arithmetic mean weighting and the upstream weighting schemes the absolute permeability, k, is weighted using the harmonic mean weighting scheme, but the relative permeability is weighted using the appropriate equation shown in Figure 21.

The same basic problem was solved using all three weighting schemes; the problem specifications were slightly different from those used earlier. The results for the liquid saturation transients in the fracture and the adjacent rock matrix (0.5 mm away from the fracture)

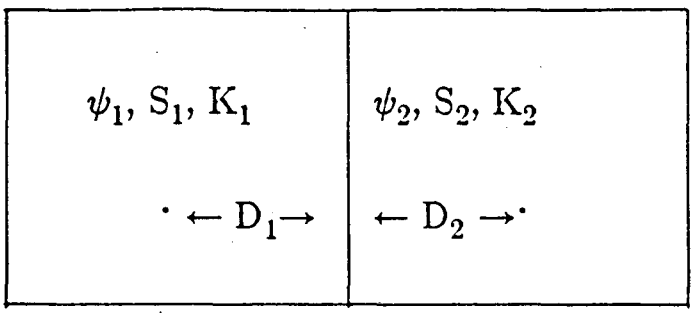

$$\text{Harmonic mean weighting :} \quad K_{1,2} = \frac{D_1 + D_2}{\frac{D_1}{K_1} + \frac{D_2}{K_2}}$$

$$\text{Arithmetic mean weighting :} \quad K_{1,2} = \frac{D_1 \times K_1 + D_2 \times K_2}{D_1 + D_2}$$

$$\text{Upstream weighting :} \quad K_{1,2} = \begin{cases} K_1 & \text{if} \quad \psi_1 > \psi_2 \\ K_2 & \text{if} \quad \psi_2 > \psi_1 \end{cases}$$

Figure 21. Formulae used for computing the permeabilities at the interfaces of the gridblocks.

using the upstream weighting scheme are shown in Figures 22 and 23, respectively. In this case the moisture front migrates about 42.5 m down the fracture during the 4.5 minute drilling period, and again the fracture recovers very rapidly. The moisture front also extends about 42.5 m in the adjacent rock matrix elements during drilling, with a recovery similar to that shown for the earlier cases.

The results obtained using the arithmetic mean weighting scheme are shown in Figures 24 and 25.

The water front moves down the fracture about 30 m during 4.5 minutes of drilling, and after one year of recovery the liquid saturation differs by less than 1 percentage point from the initial saturation.

The results obtained using the harmonic mean weighting scheme differ substantially from those obtained using the upstream and the arithmetic mean weighting schemes, as shown in Figure 26. In this case the front moves only about 3 m down the fracture and the adjacent rock matrix after 31 days of drilling. The reason for this is the relatively low mobility obtained at interfaces when the harmonic mean weighting is used. Unlike the other two weighting schemes, the harmonic mean weighting scheme puts most weight upon the downstream permeabilities, which are low due to the lower liquid saturations. Thus, the moisture front cannot move down to the next grid block until after the grid block at the edge of the front becomes fully saturated. The low fluid mobility of the harmonic mean weighting scheme allows very little liquid water to enter the fracture from the constant head boundary in comparison to the other weighting schemes.

It is expected that the different weighting schemes will yield similar results when an extremely fine grid is used. This should be tested in future simulations. However, significant differences were also obtained by USGS in their simulations using a rather fine grid and different weighting methods (5 cm grid blocks; E. Kwicklis, personal communication, 1987).

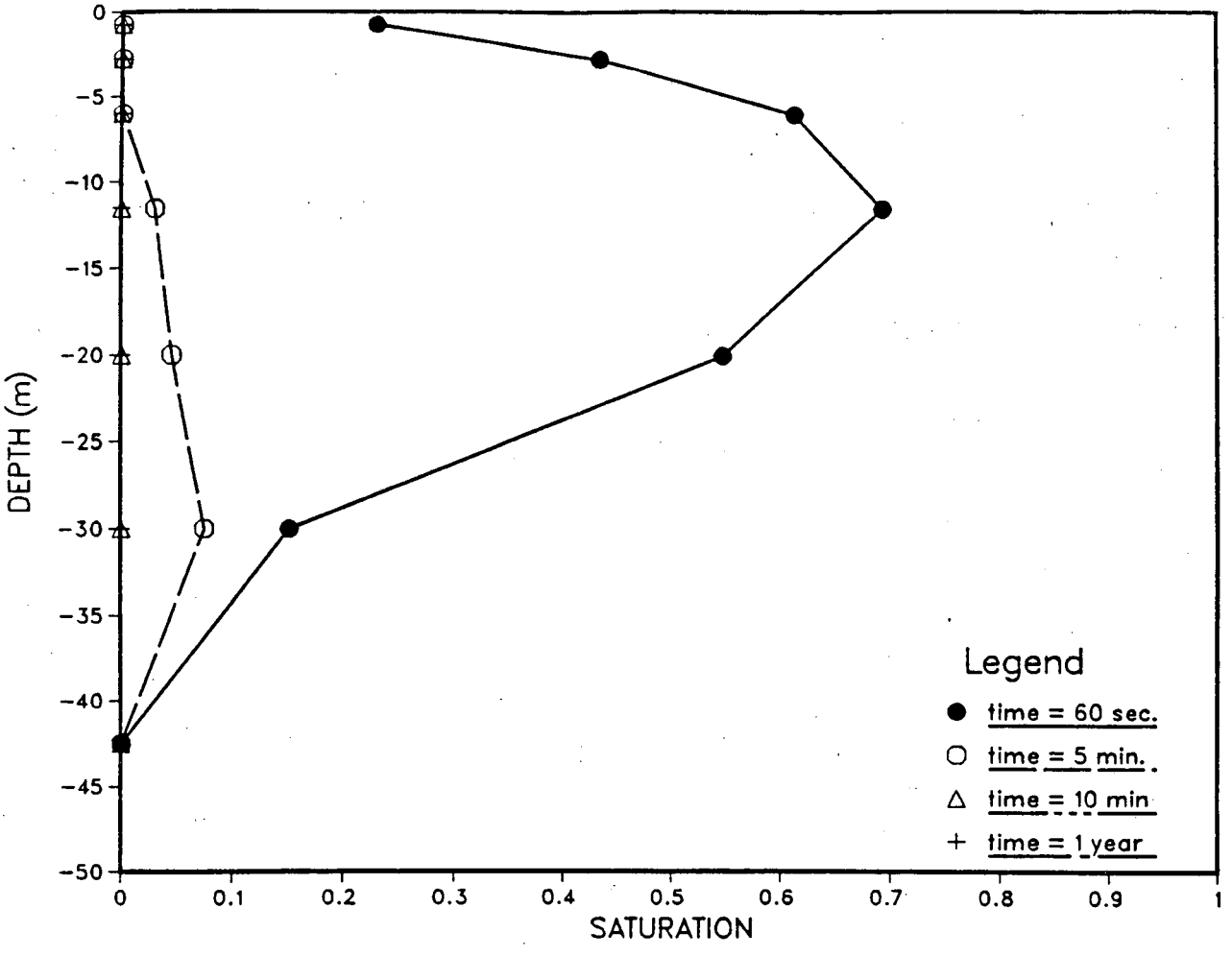

Figure 22. Upstream weighting: Liquid saturation in the fracture for various recovery times.

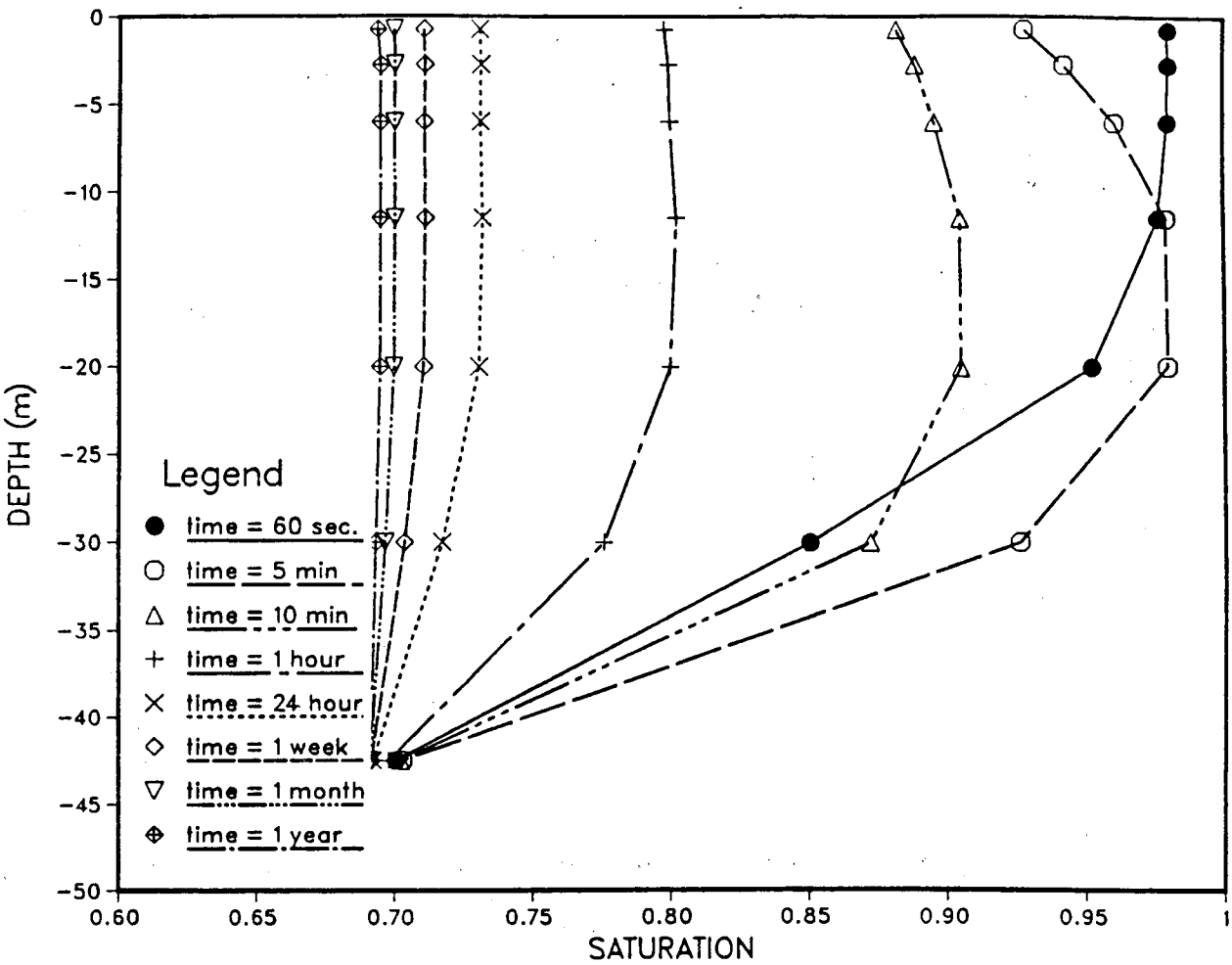

Figure 23. Upstream weighting: Liquid saturation in the matrix (0.5 mm from the fracture) for various recovery times.

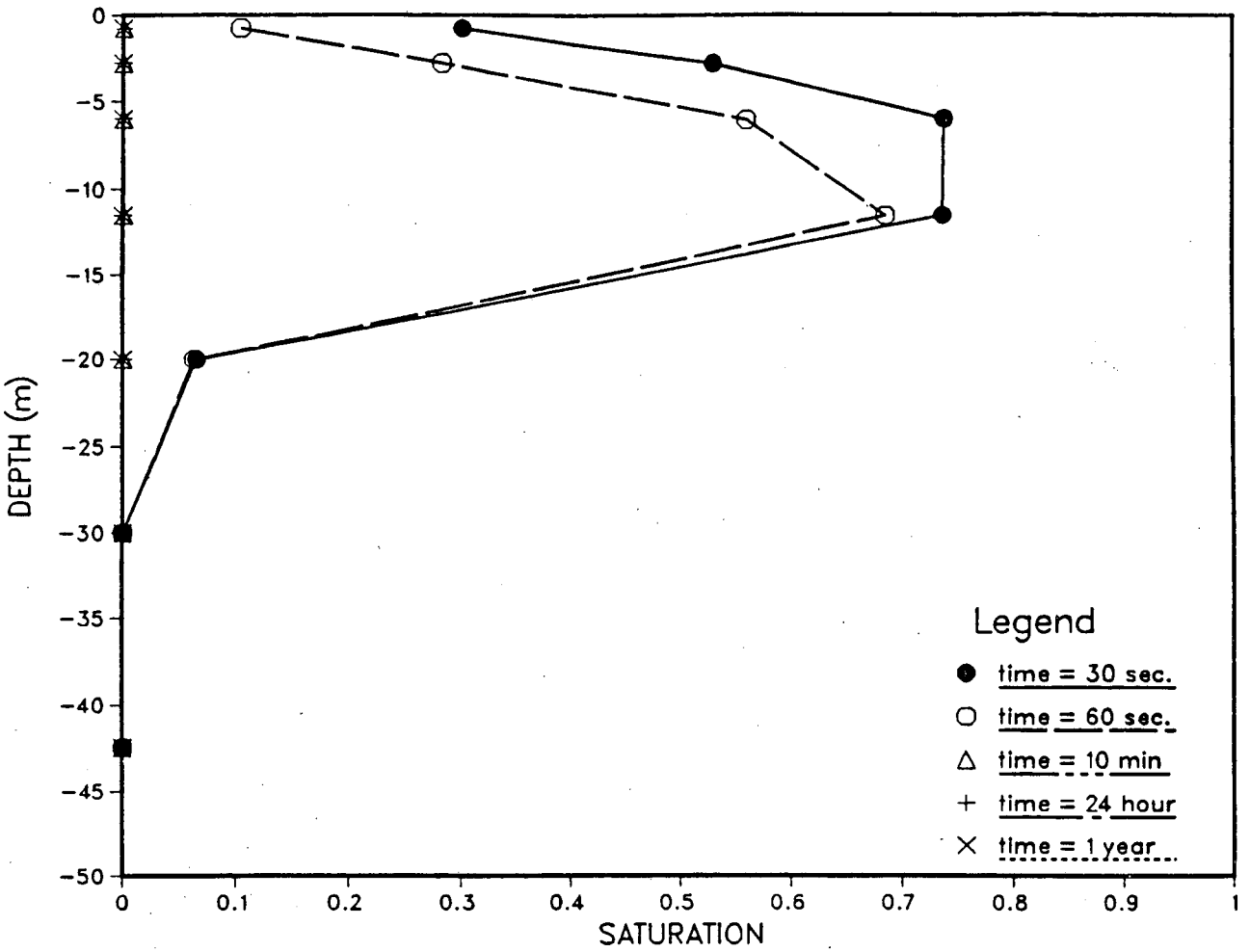

Figure 24. Arithmetic mean weighting: Liquid saturation in the fracture for various recovery times.

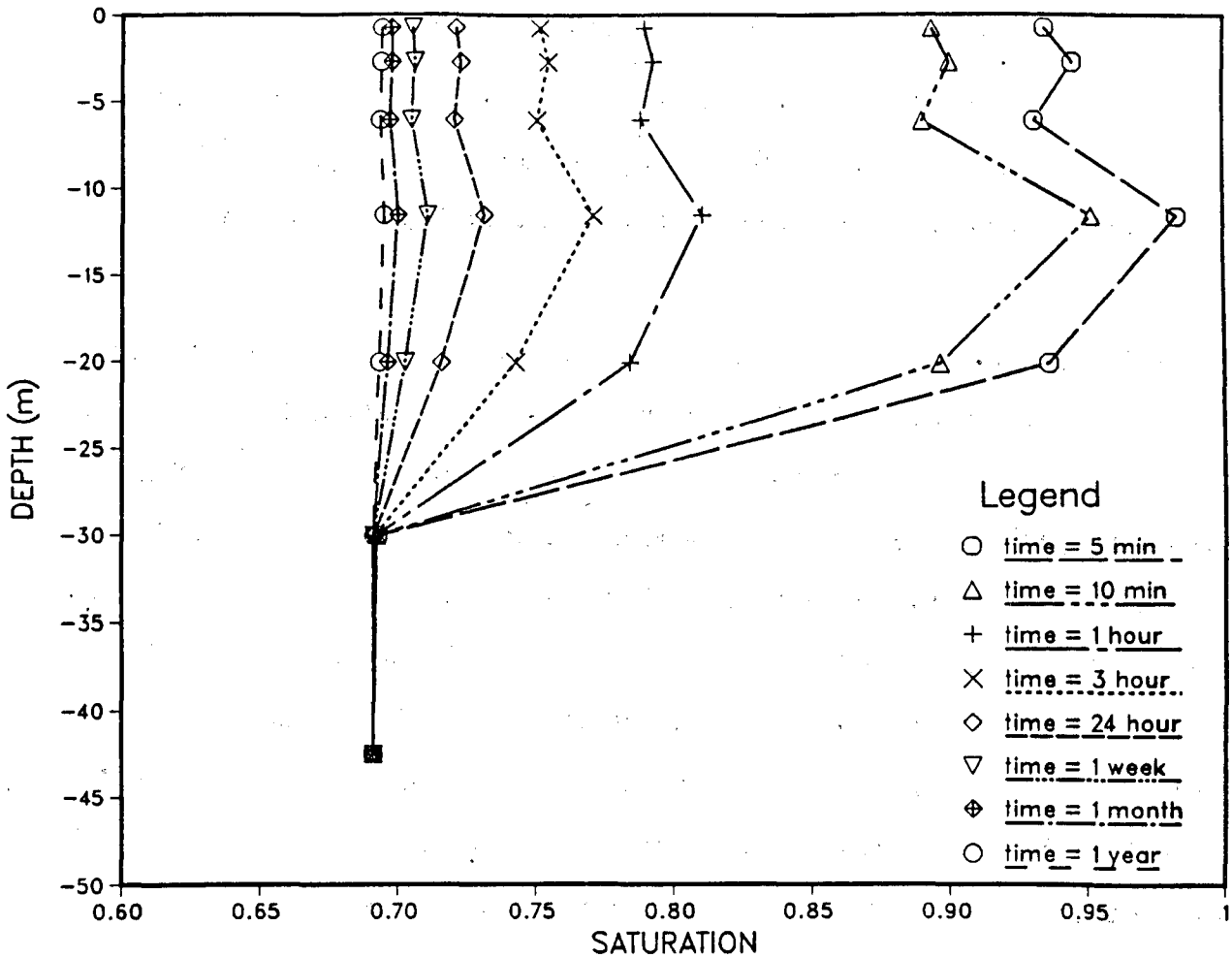

Figure 25. Arithmetic mean weighting: Liquid saturation in the matrix (0.5 mm from the fracture) for various recovery times.

Horizontal Moisture Migration

The horizontal moisture migration due to liquid water drilling of a borehole or wet-mining of a shaft room was briefly investigated. Two different cases were considered with the same numerical grid that was used in the investigation of vertical fluid flow. In these cases, however, the system was rotated 90° so that the fracture is horizontal.

Gravity effects were turned off so that the only driving forces for moisture migration were capillary pressure gradients. A water head of 20 m was imposed at one end of the system for a total time of one hour. Uniform initial conditions with a capillary pressure of -0.97 bars were specified.

In the first set of simulations the parameter values given in Table 1 were used with the USGS characteristic curves. Figures 27 through 29 show the results obtained from these simulations. Figures 27 and 28 show that after 12.25 minutes of drilling the liquid water front has advanced about 11.5 m in both the fracture and adjacent rock matrix elements. In comparison, for the vertical fracture case (Figures 4 and 5) the moisture front migrates about 20 m in the rock matrix adjacent to the fracture. These results indicate that for this problem the capillary pressure forces are at least comparable to the gravity force; this can be verified by comparing the magnitudes of the two forces using Darcy's law. The moisture redistribution during the recovery period is also similar for the two cases (with and without gravity), with the matrix liquid saturation being at most about one percentage point higher than the initial saturation after a one year recovery period.

A second set of simulations was conducted using a considerably smaller fracture with a volumetric aperture of 0.05 mm and a hydraulic aperture of 0.01 mm. The volumes and surface areas of the fracture elements were computed based upon the volumetric aperture and the fracture permeability based on the hydraulic aperture. The results from these simulations are shown in Figures 30, 31 and 32. In this case the liquid water front only migrates into the first grid block after 1 hour of drilling. The subsequent recovery is also more rapid with the liquid saturation in the matrix blocks closest to the constant head boundary being within 1.2

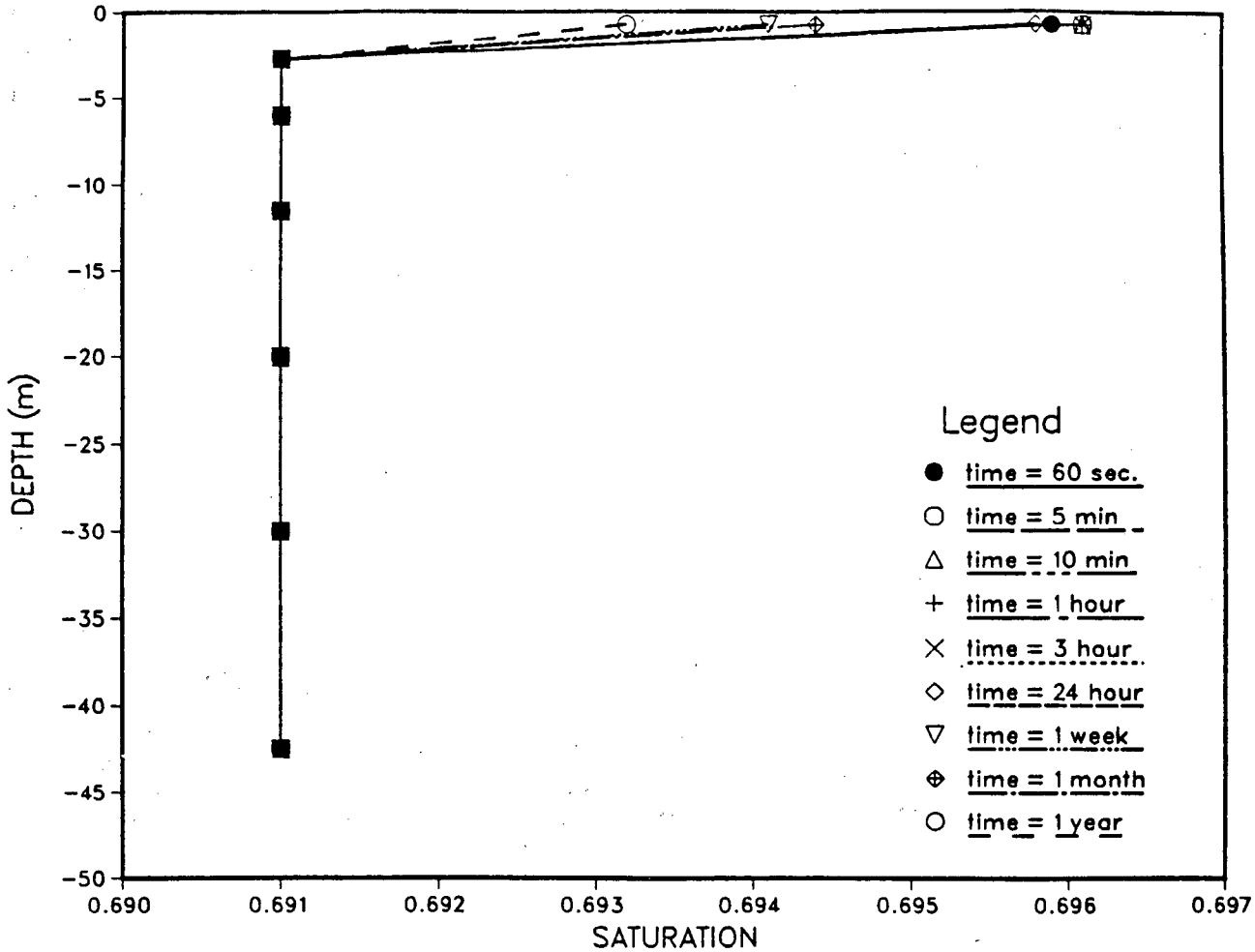

Figure 26. Harmonic mean weighting: Liquid saturation in the matrix (0.5 mm from the fracture) for various recovery times.

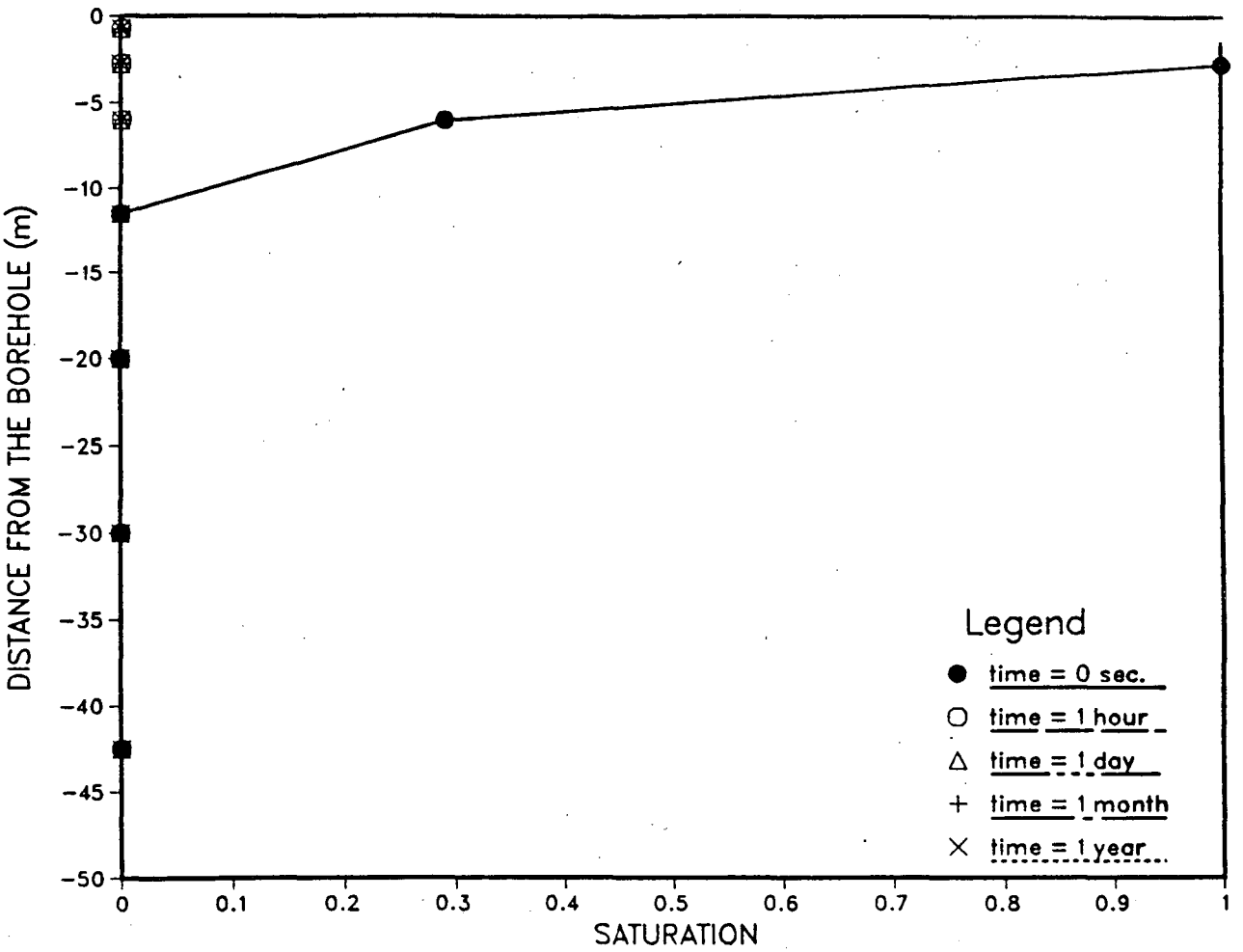

Figure 27. Horizontal fracture model (large aperture): Liquid saturation in the fracture for various recovery times.

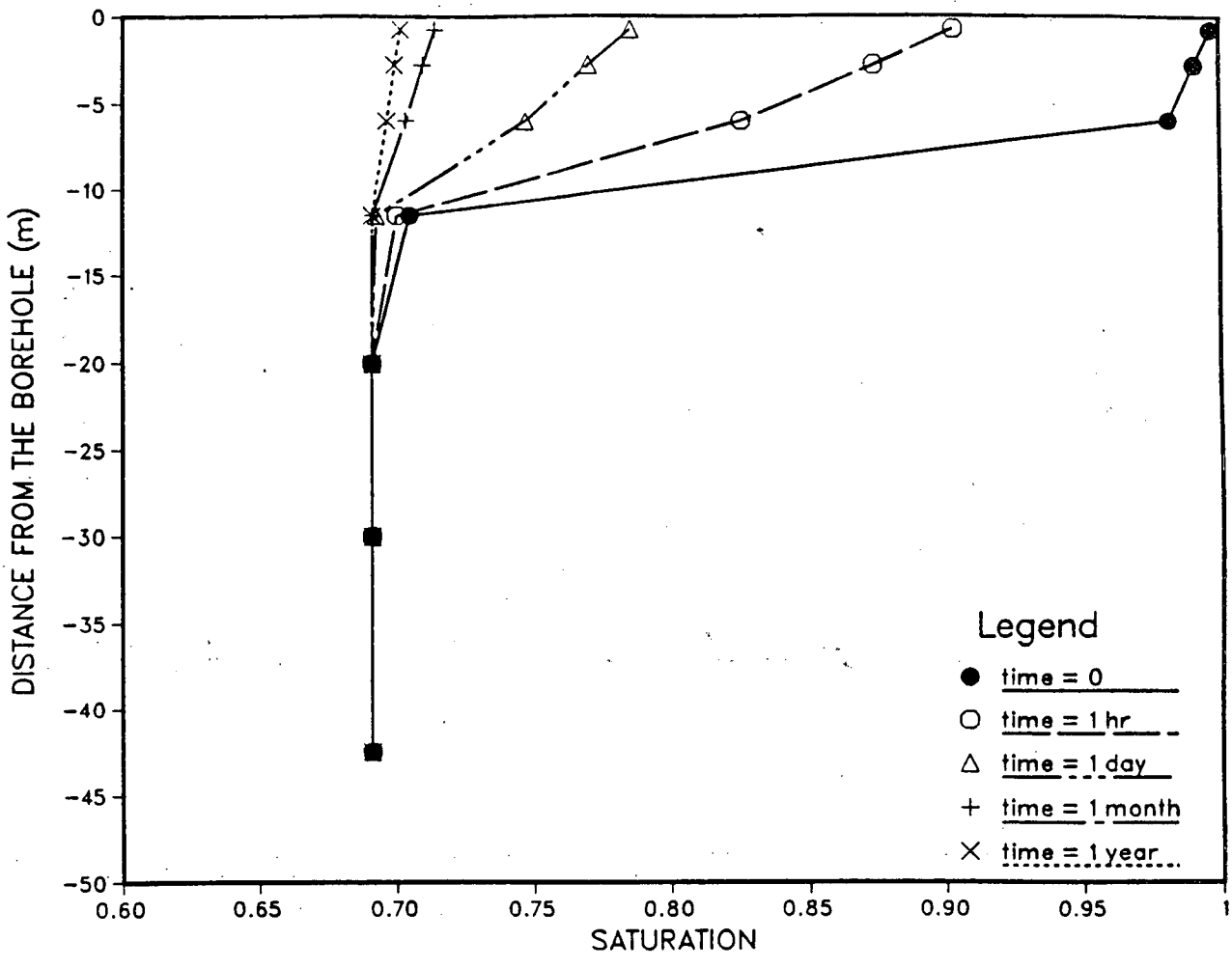

Figure 28. Horizontal fracture model (large aperture): Liquid saturation in the matrix (0.5 mm from the fracture) for various recovery times.

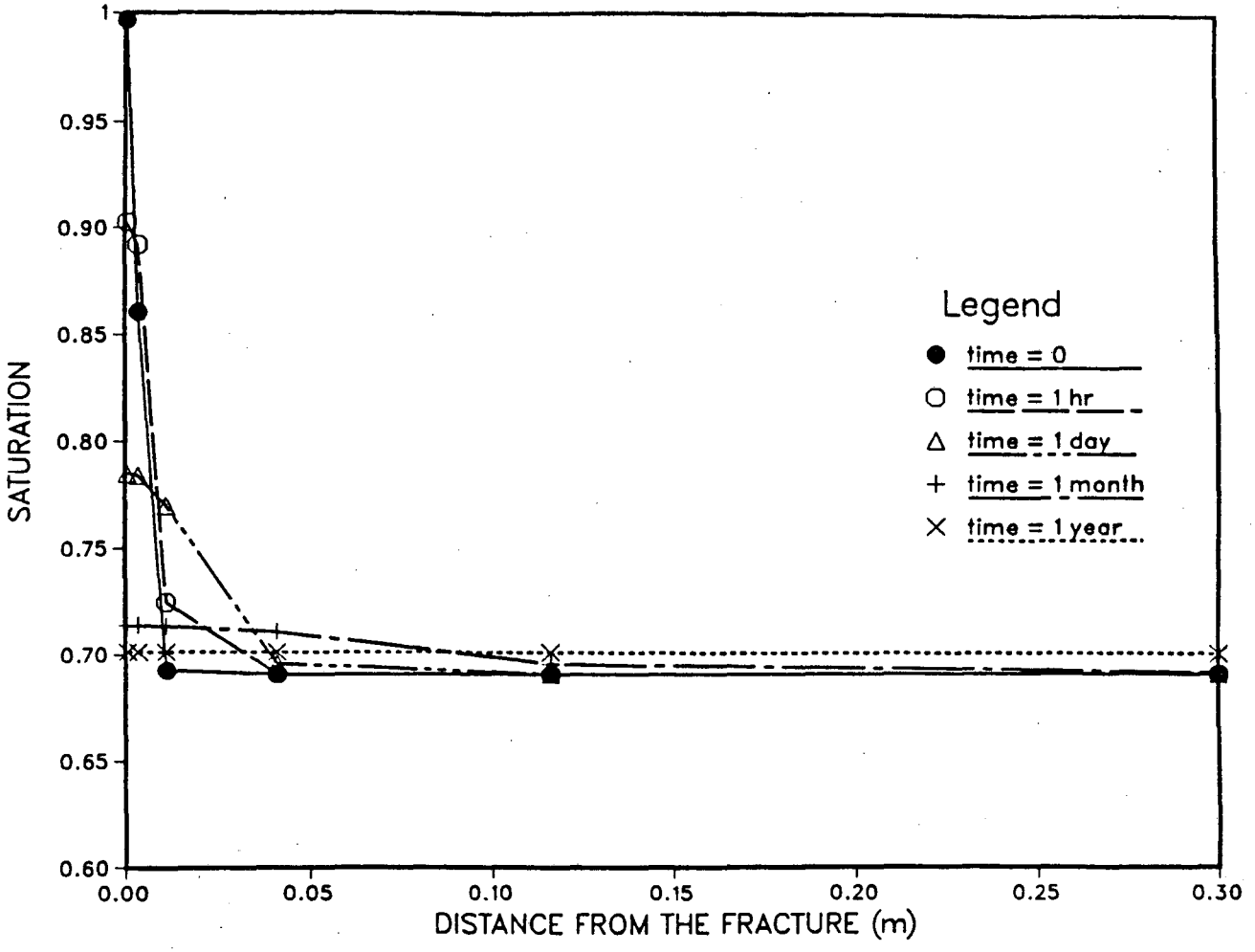

Figure 29. Horizontal fracture model (large aperture): Liquid saturation in the matrix (0.75 m from the borehole) for various recovery times.

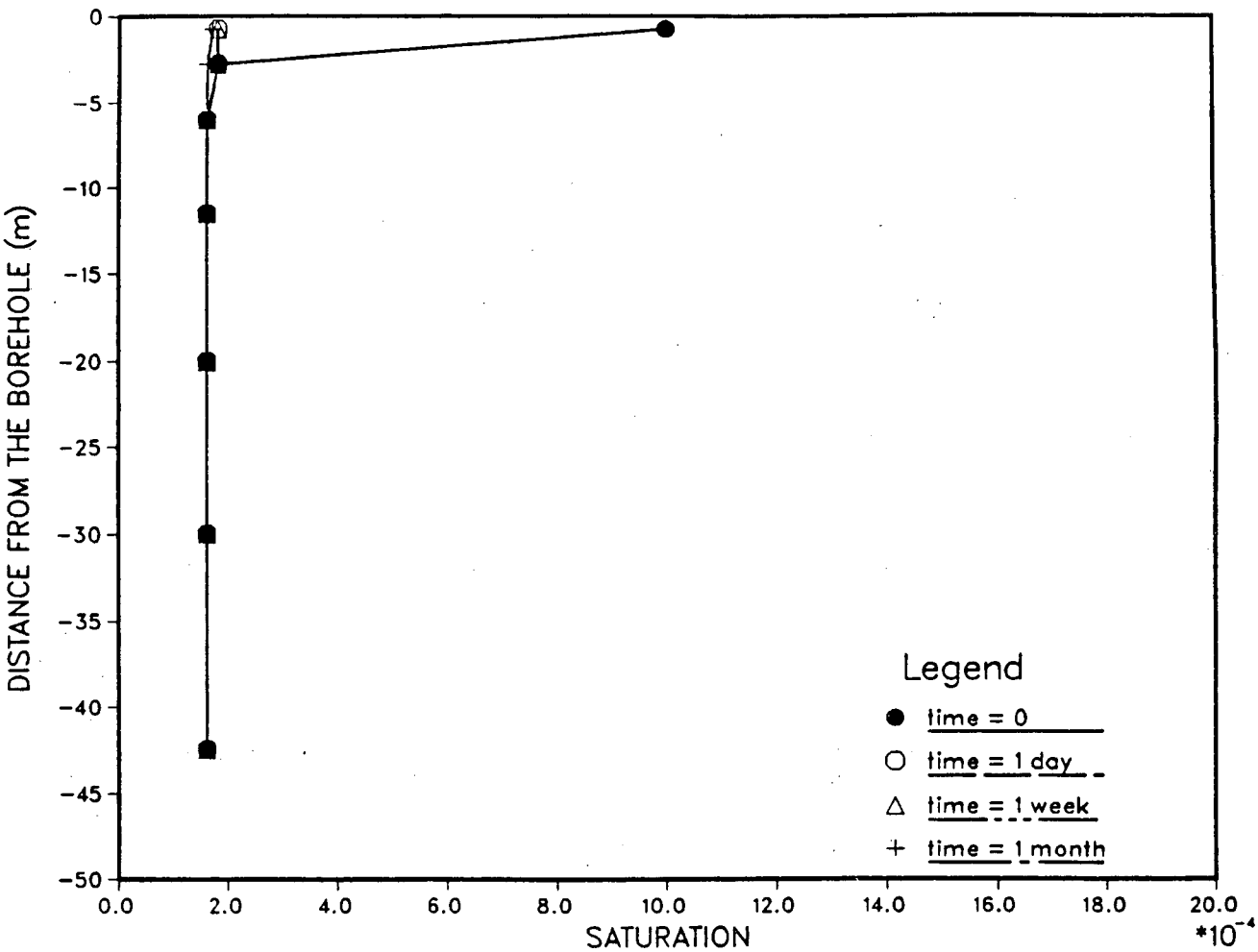

Figure 30. Horizontal fracture model (small aperture): Liquid saturation in the fracture for various recovery times.

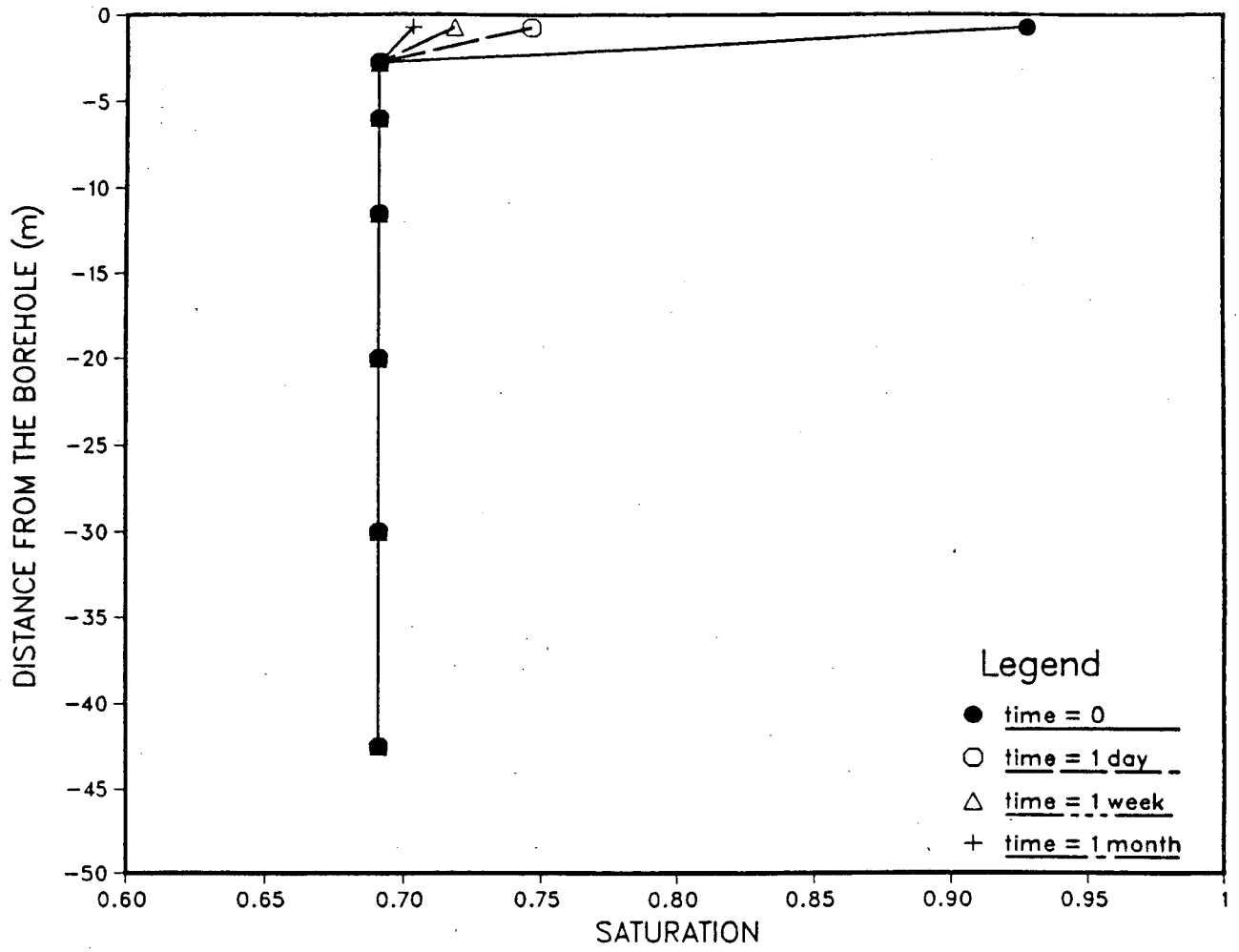

Figure 31. Horizontal fracture model (small aperture): Liquid saturation in the matrix (0.5 mm from the fracture) for various recovery times.

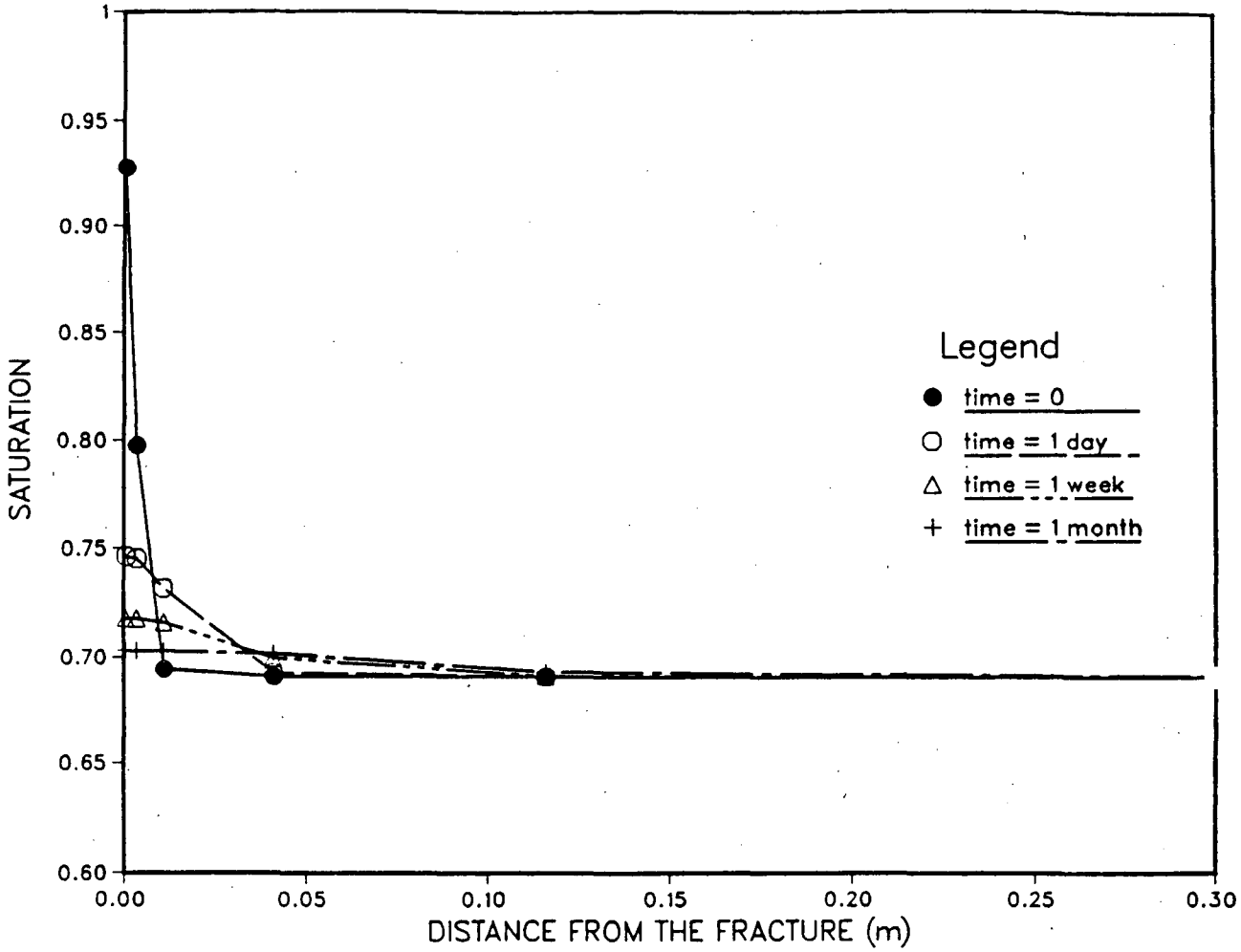

Figure 32. Horizontal fracture model (small aperture): Liquid saturation in the matrix (0.75 m from the borehole) for various recovery times.

percentage points from the initial value after a one-month recovery.

Air Drilling

A brief study was conducted on the effects of air drilling on moisture conditions in nearby fractures and rock matrix blocks. Again the grid shown in Figure 1 and the parameter values given in Table 1 (with the USGS characteristic curves) were used. In this case, a 2 bar air pressure condition was specified at the top of the system. The relative permeability to air, k_{rg}, was assumed to be $1-k_{rl}$ for all saturations. The air drilling was assumed to last for a period of 12.25 minutes. The temperature increase of the air due to drilling was not considered in the simulations, although that may lead to drying of matrix block surfaces (E. Kwicklis, personal communication, 1988). Figures 33, 34 and 35 show the moisture conditions in the fracture, in the rock matrix elements adjacent to the fracture, and in the interior of the rock matrix, respectively, immediately after drilling ceased and during the recovery. Figures 36 through 38 show the air pressure transients in the various parts of the system during the recovery period.

The liquid saturation transients shown in Figures 33 through 35 suggest that only small changes in liquid saturation will occur as a result of air drilling. The maximum decrease in liquid saturation in the matrix is about 0.005 in a matrix element adjacent to the fracture. After one day of recovery the liquid saturations have practically recovered in both the fracture and the rock matrix. In the interior of the rock matrix no significant changes in the liquid saturation are observed (Figure 35). Figures 36 through 38 show that large air pressure gradients develop in the fracture and the adjacent rock matrix elements during air drilling. The pressure pulse moves quickly within the fracture to the constant pressure element at the bottom of the system (depth of 50 m). In the interior of the matrix significant air pressure changes are only observed down to a depth of 3 m (Figure 38). The air pressure recovery is rapid, with near-initial conditions reached after about one day. In the case studied the inflowing air was near-saturated with water, but the results would not differ greatly if "dry" air was used.

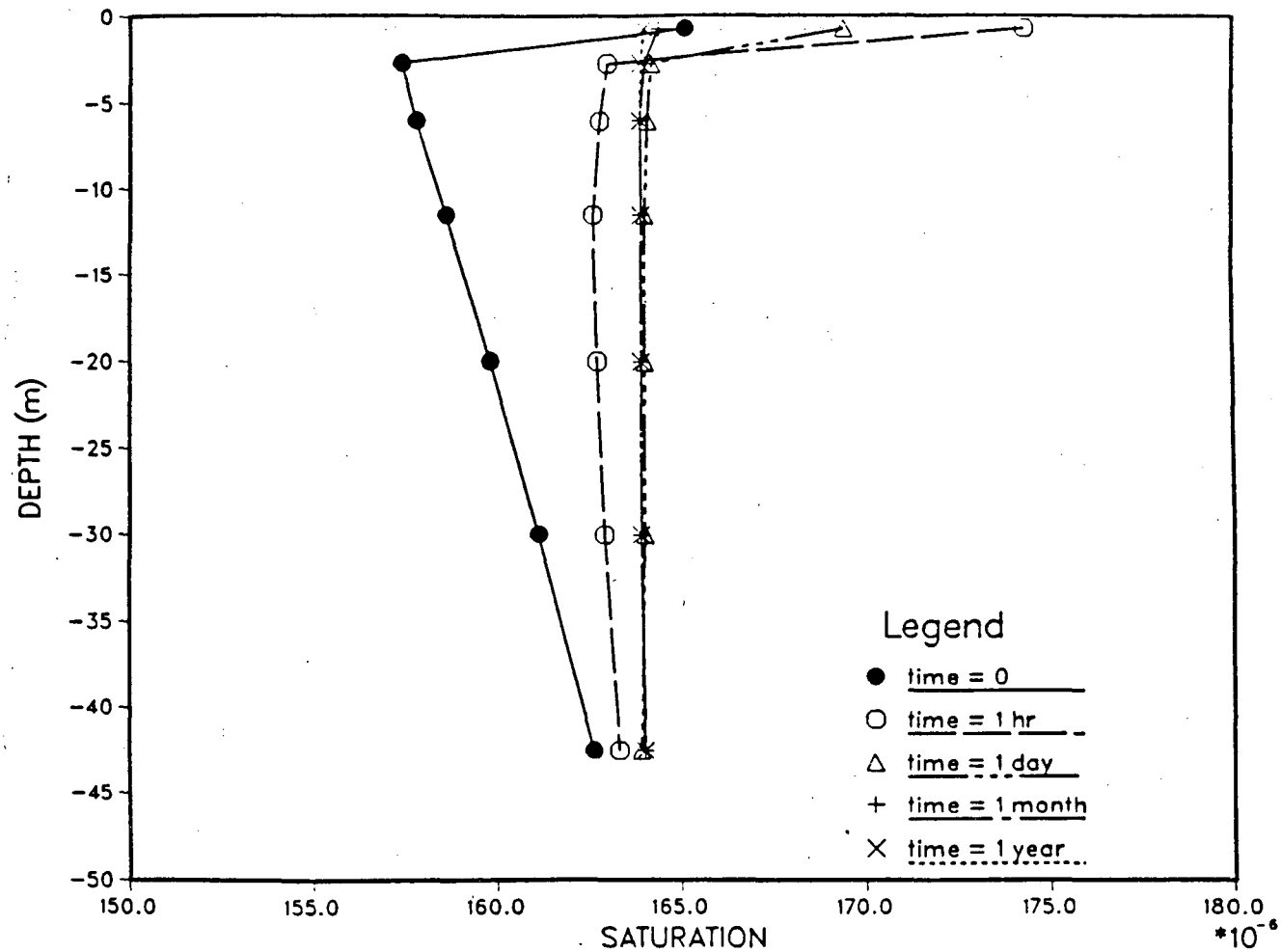

Figure 33. Drilling with air: Liquid saturation in the fracture for various recovery times.

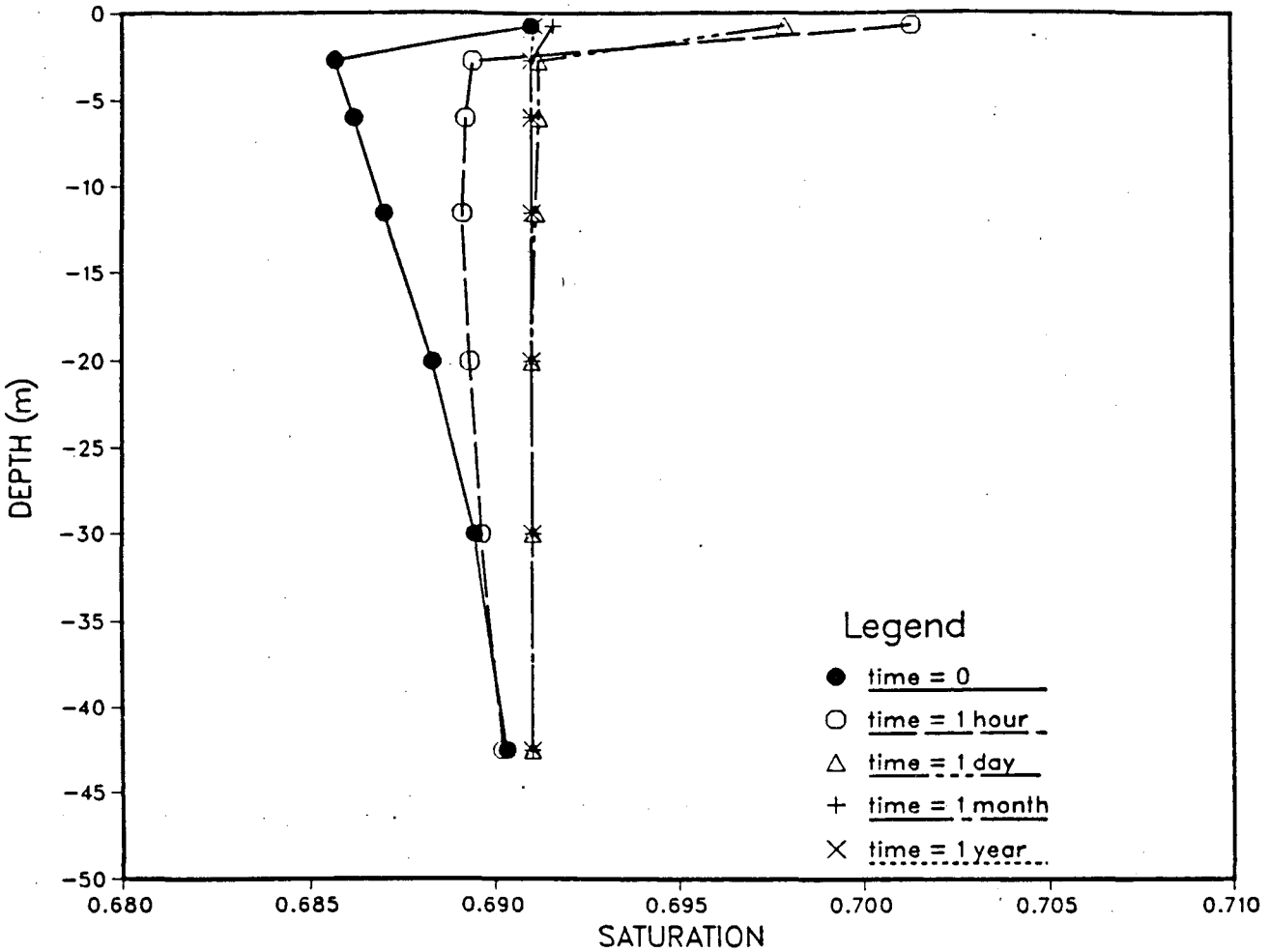

Figure 34. Drilling with air: Liquid saturation in the matrix (0.5 mm from the fracture) for various recovery times.

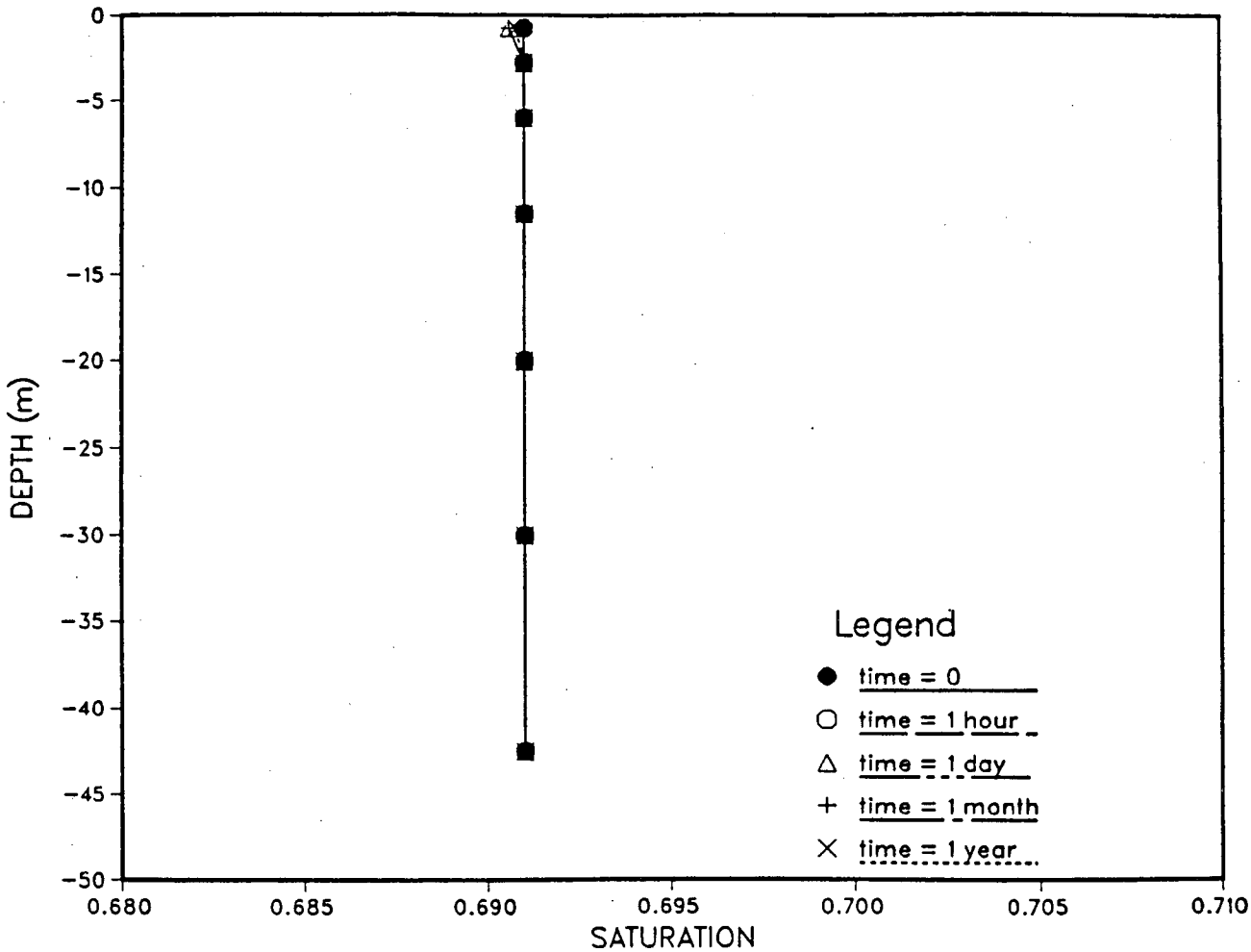

Figure 35. Drilling with air: Liquid saturation in the center of the matrix for various recovery times.

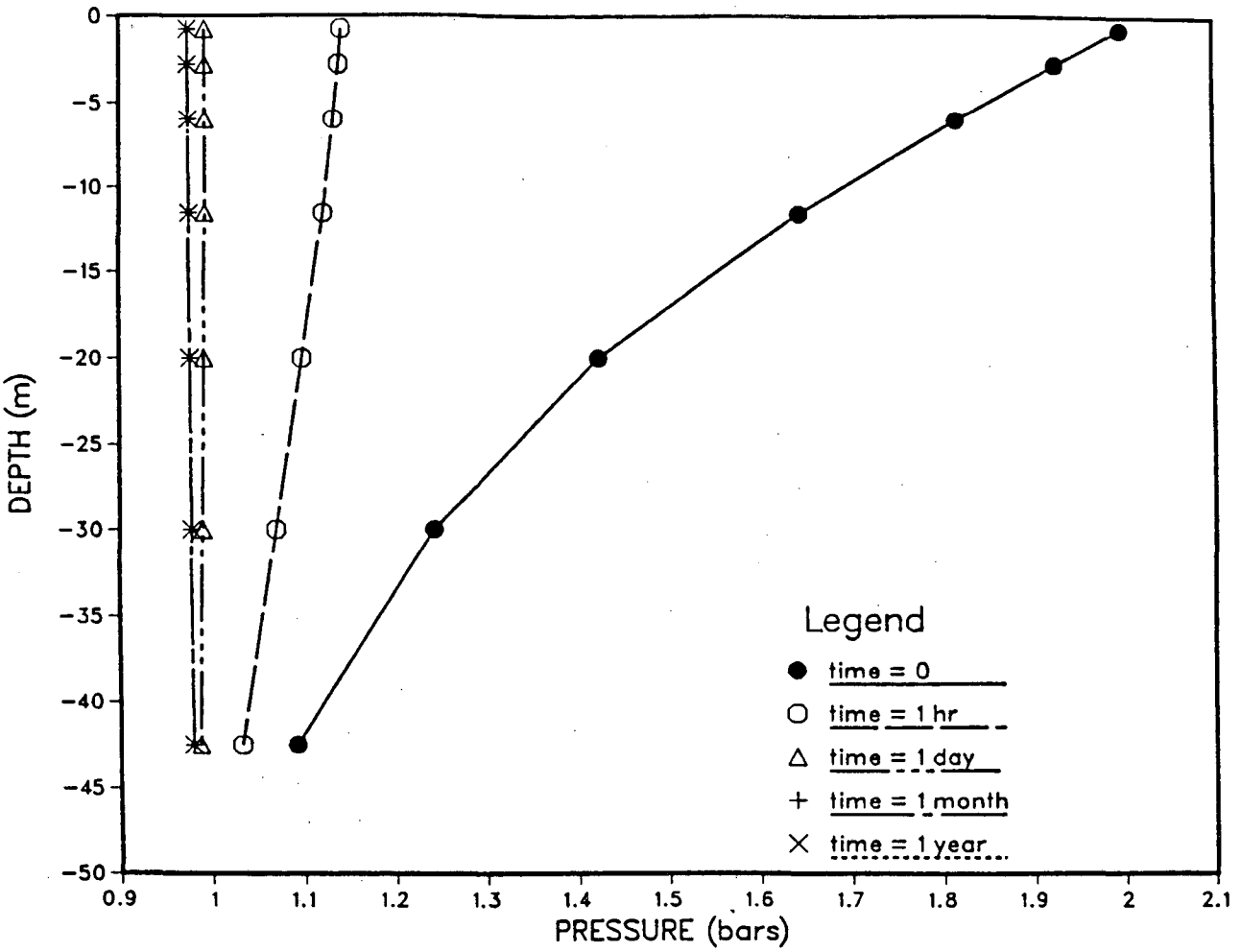

Figure 36. Drilling with air: Air pressure in the fracture for various recovery times.

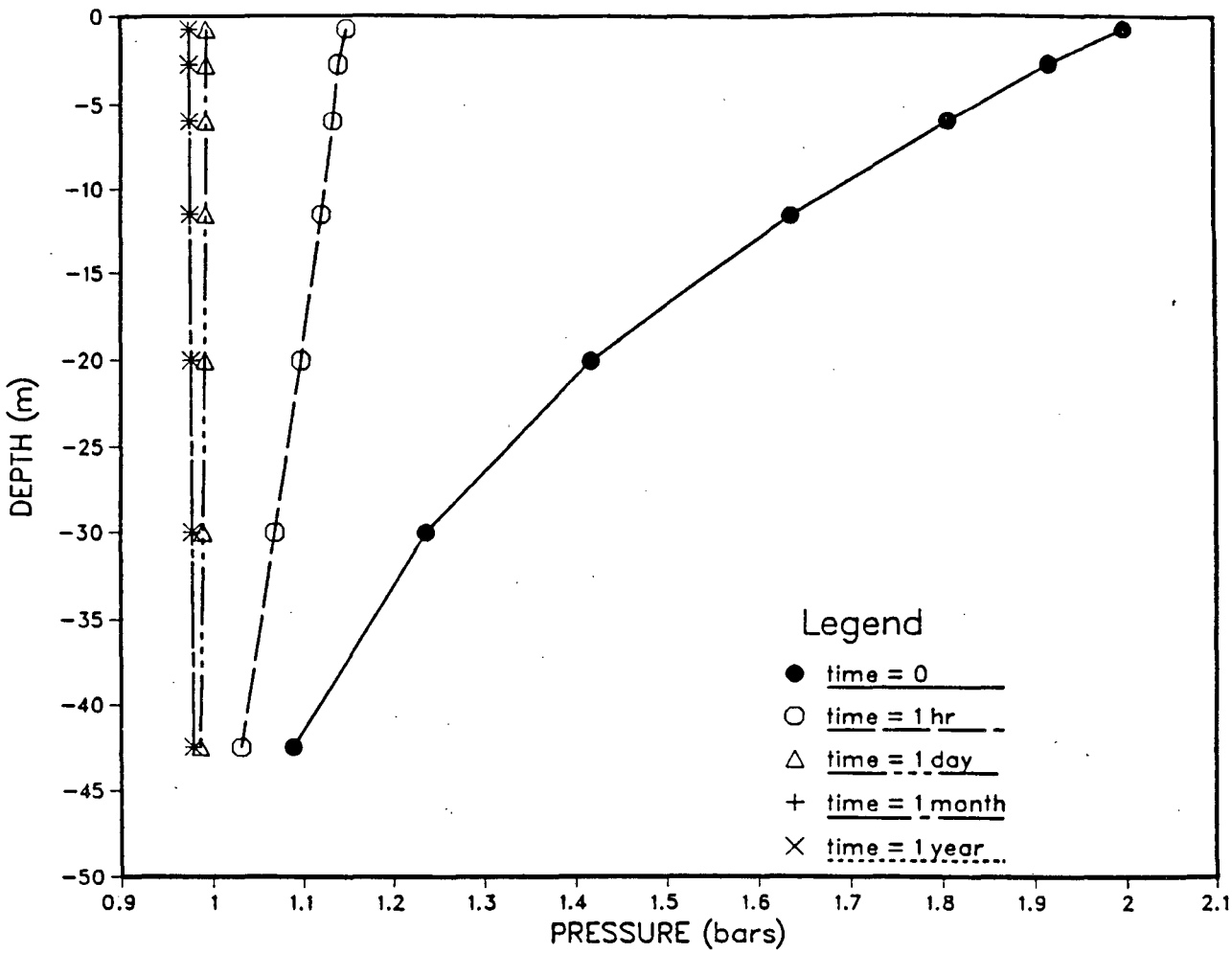

Figure 37. Drilling with air: Air pressure in the matrix (0.5 mm from the fracture) for various recovery times.

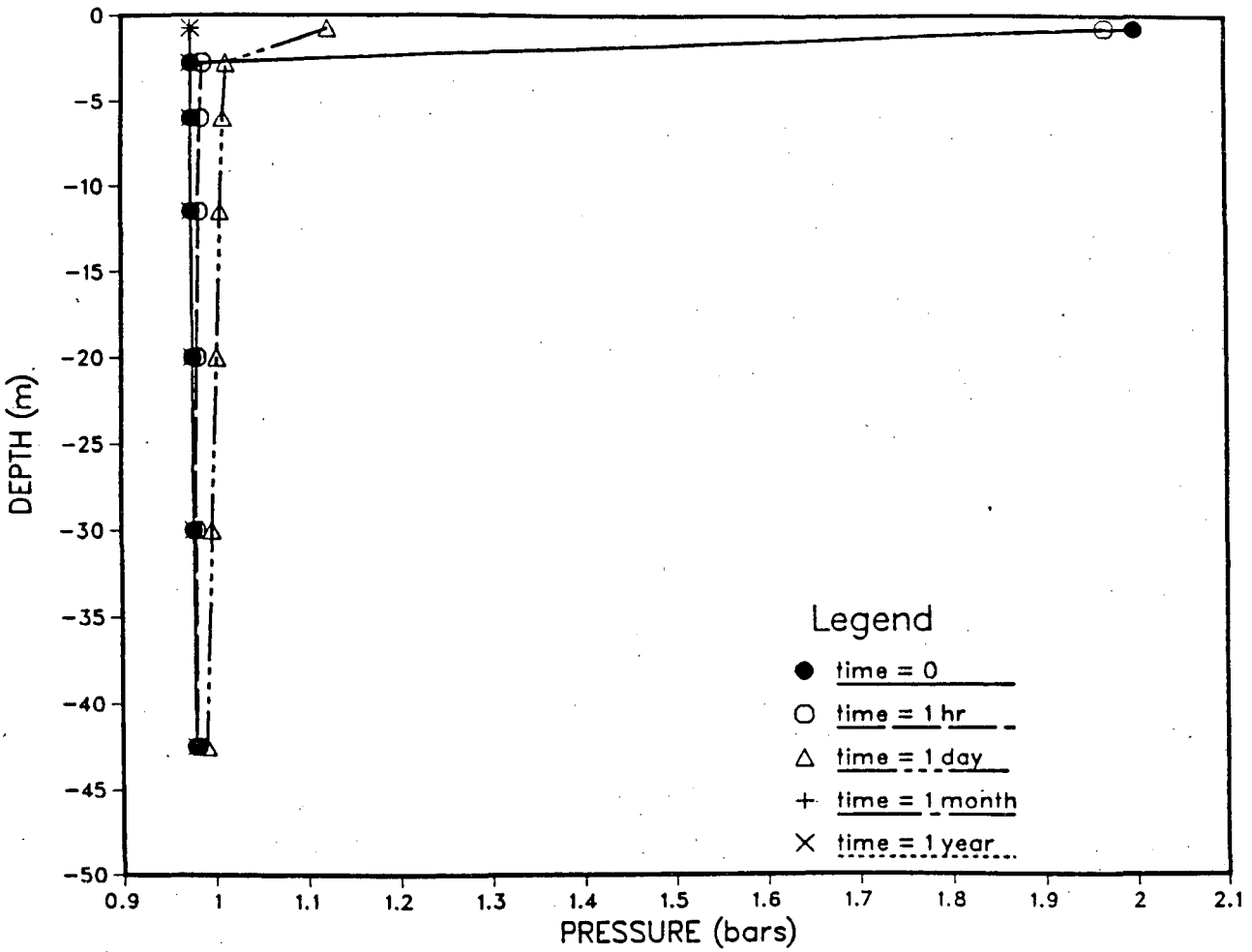

Figure 38. Drilling with air: Air pressure in the center of the matrix for various recovery times.

SUMMARY

Numerical simulation studies were carried out to address the effects of air and liquid water drilling on the time-dependent moisture conditions in nearby fractures and rock matrix blocks. A very coarse numerical grid was used to obtain first order estimates of changes in moisture conditions that result from an imposed head of water (or air) for some (drilling) period and from the subsequent redistribution of the moisture.

For the parameter values used the moisture front migrated tens of meters down the fractures and in the rock matrix adjacent to the fractures. The most critical parameter is the aperture of the fractures and the corresponding fracture permeability. If the effective fracture aperture is tens of microns rather than the assumed value of 100 microns, the moisture front is likely to advance considerably less during the assumed 12.25 minutes drilling period. The results obtained suggest that the lateral (horizontal) moisture migration may be about half the vertical one, for the parameter values considered and the conceptual model used.

The moisture redistribution in the fracture following liquid water drilling occurs in minutes or hours, with the water being drawn into the matrix and very little further advancement of the moisture front. The moisture redistribution within the matrix takes a much longer time, on the order of years. After one year of recovery the matrix saturation is fairly uniform at a given depth and up to one to two percentage points higher than the initial liquid saturation. For the characteristic curves used this corresponds to a diference of about 10 to 20% in the relative permeability of the liquid phase. When hysteresis in the capillary pressure-liquid saturation relationship for the matrix is considered, the recovery may be considerably slower and result, in the vicinity of the fractures, with considerably larger differences between the matrix liquid saturations after one year of recovery and the initial values. For the non-hysteretic case the USGS and Sandia characteristic curves give similar results for the problem solved. Limited sensitivity studies of grid effects suggested that they are secondary in importance for the purposes of this study as similar results are obtained with two grids with different element sizes.

The results for the case involving air drilling, assuming saturated air and isothermal conditions, suggest that much less disturbance in the moisture conditions of nearby fractures and rock matrix blocks will occur. Slight changes in liquid saturations occur in the fractures and the adjacent rock matrix elements with rapid recovery within a time frame of hours or days after drilling ceases.

REFERENCES

Klavetter, E. A. and Peters, R. R., 1986. Fluid flow in a fractured rock mass. Rep. SAND85-0855, Sand. Nat. Lab., Albuquerque, N. M. 55 pp.

Kool, J. B. and Parker, J. C., 1987. Development and evaluation of closed-form expressions for hysteretic soil hydraulic properties. *Water Resources Research, 23,* (1) 105-114.

Kwicklis, E. and Hoxie, D., 1987. An estimation of the influence of drilling-induced moisture perturbations in an hypothetical infiltration test. Draft report. U.S. Geological Survey, Denver, CO.

Montazer, P., Harrold, P.E., Snow, D. T., and Trautz, R. C., 1987a. Effects of dry versus wet mining in portions of the main test horizons of the exploratory shaft at Yucca Mountain. Draft Report. U.S. Geological Survey, Denver, CO.

Montazer, P., Harrold, P. E., Thamir, F., Naugle, G., Kwicklis, E. and Hoxie, D., 1987b, Determination of hydraulic properties of partially saturated fractured rocks. Report in preparation. U.S. Geological Survey, Denver, CO.

Montazer, P. and Wilson, W. E., 1984. Conceptual hydrologic model of flow in the unsaturated zone, Yucca Mountain, Nevada. U. S. Geological Survey Water Resources Investigation Report 84-4345, 55 pp.

Mualem, Y., 1984. A modified dependent domain theory of hysteresis. *Soil Science, 137,* (5) 283-291.

Niemi, A., Bodvarsson, G. S., and Montazer, P., 1987. Preliminary capillary hysteresis simulations for fractured rocks. Rep. LBL-23593. Lawrence Berkeley Laboratory, Berkeley, Ca., 80 pp.

Peters, R. R. and Gauthier, J. H., 1986. NNWSI Hydrologic Analysis No. 8.

Pruess, K., 1983. GMINC-a mesh generator for flow simulations in fractured reservoirs. Rep. LBL-15227. Lawrence Berkeley Laboratory, Berkeley, Ca., 64 pp.

Pruess, K., 1987. TOUGH-users guide. Rep. LBL-20700. Lawrence Berkeley Laboratory, Berkeley, Ca., 84 pp.

Rulon, J., Bodvarsson, G. S. and Montazer, P., 1986. Preliminary numerical simulations of groundwater flow in the unsaturated zone, Yucca Mountain, Nevada. Rep. LBL-20553. Lawrence Berkeley Laboratory, Berkeley, Ca., 88 pp.

Travis, B. J., Hodson, S. W., Nuttal, H. E., Cook, T. L. and R. S. Rundberg, 1984. Preliminary estimates of water flow and radionuclide transport in Yucca Mountain, Los Alamos Report LA-UR-844-40, 75 pp.

Wang, J. S. Y. and Narasimhan, T. N., 1985. Hydrological mechanisms governing fluid flow in a partially saturated, fractured, porous medium, *Water Resources Research, 21,* (12) 1861-1874.

Wang, J. S. Y. and Narasimhan, T. N., 1986. Hydrologic mechanisms governing partially saturated fluid flow in fractured welded units and porous nonwelded units at Yucca Mountain, Lawrence Berkeley Laboratory Report LBL-21022, Sandia National Laboratory Report, SAND85-7114. Lawrence Berkeley Laboratory, University of California, Berkeley, CA 94720.

LAWRENCE BERKELEY LABORATORY
TECHNICAL INFORMATION DEPARTMENT
UNIVERSITY OF CALIFORNIA
BERKELEY, CALIFORNIA 94720